



Landscape evolution of Mesozoic sediments in the Andamooka area, incorporating remotely sensed ASTER data to facilitate future mineral exploration

Mathew Kavanagh

Geology and Geophysics, School of Earth and Environmental Sciences
University of Adelaide, Adelaide SA 5005 Australia

Supervisor: Dr Robert Dart

Co-supervisor: Dr Steve Hill

2011

i. Abstract

Regolith and sedimentary material overlying potentially enriched basement, is an ever-present obstacle in the highly prospective Olympic iron-oxide copper gold (IOCG) Province, South Australia. The Eromanga Basin, composed of Mesozoic sediments - Algebuckina Sandstone, Cadna-owie Formation and Bulldog Shale - overlies the northern extent of the Stuart Shelf, including the Olympic Dam IOCG province. The closest surface exposures of these sediments to Olympic Dam, is around the opal mining town of Andamooka. The formation and distribution of the precious opal has been previously linked to fluctuating water tables. However, oxidation of pyrite by fluctuating water table height, caused by intracontinental extensional faulting in the area, provides an enhanced interpretation linking opal distribution with the presence of jasper and silcrete lag. Extensional fault boundaries were identified through contrasting regolith and landform components observed from field mapping and remote sensing imagery. ASTER band ratios and relative absorption-band depth ratios complimented field observations with ratios primarily useful in distinguishing high reflectance homogenous mineral groups e.g. opal diggings and sand dunes. A regolith-landform map and digital elevation model over the area identifies the contrasting units, with opal diggings (digitised from ASTER imagery) strongly associated with higher elevations.

The potential for secondary economic mineralisation is proposed for the Andamooka area. A source material (Olympic IOCG Province), transport mechanism (extensional duplex faulting), and potential trap rock (REDOX boundaries and varying

permeability of Mesozoic units) all contributed to a prospective exploration model for the area.

Key words: Andamooka; Eromanga Basin; Mesozoic sediments; Bulldog Shale; Algebuckina Sandstone; Cadna-owie Formation; ASTER satellite imagery; opal

Table of Contents

i. Abstract.....	2
1. Introduction.....	6
1.1 Project aims.....	6
1.2 Geological setting	6
1.2.1 Algebuckina Sandstone.....	8
1.2.2 Cadna-owie Formation.....	10
1.2.3 Bulldog Shale.....	13
1.3 Regolith and landscape evolution	15
1.4 Remote sensing background	17
2. Methods.....	18
2.1 Regolith-landform mapping.....	18
2.2 Soil diagnostic tests.....	19
2.3 Hylogger analysis.....	20
2.4 ASTER analysis using band ratio processing	21
2.5 Supervised classification using combined ASTER data and field observations	23
2.6 Digital elevation model.....	23
3. Results	24
3.1 Regolith-landforms	24
3.2 Remote sensing imagery	28
3.3 Hylogger analysis.....	31
4. Discussion.....	32
4.1 Regolith-landform map and landscape evolution	32
4.2 ASTER analysis	38

4.3 Hylogger interpretations	40
4.4 Mineral prospectivity	40
4.5 Scope for further study.....	41
5. Conclusion	43
6. Acknowledgements	44
7. References.....	45
8. Figure captions.....	51
9. Figures.....	53
10. Tables	69

1. Introduction

1.1 Project aims

The aim of this project was to: i) construct a regolith-landform map for the Andamooka area and interpret the landscape evolution; ii) identify relationships between field observations and remotely sensed data; and iii) evaluate the mineral prospectivity of the area. This was accomplished through a combination of field and laboratory work.

The Andamooka location was selected because of its close proximity to mineralisation at Olympic Dam and the presence of Mesozoic sediments exposed at the surface. In other areas these units have been found to act as a trap for secondary mineralisation (Hill and Hore 2010). This study focuses on the surface expression and composition of the Mesozoic sediments, as they constitute part of the regolith components which blanket the mineral enrichment, causing difficulty in exploration whilst potentially hosting secondary mineralisation.

The results of this project will contribute to the Deep Exploration Technologies Cooperative Research Centre's (DET CRC) overall study of the Stuart Shelf region, with the objective of assisting exploration drilling through a better understanding of overlying cover material.

1.2 Geological setting

The Stuart Shelf in the Gawler Craton, South Australia is host to Olympic Dam, one of the world's largest known iron oxide copper gold (IOCG) deposits. Additional

IOCG type prospect have been discovered in the surrounding area at Acropolis, Wirrda Well, Oak Dam and Prominent Hill, demonstrating the prospectivity of the area (Belperio *et al.* 2007; Skirrow and Davidson 2007). Despite these discoveries, Prominent Hill is currently the only deposit considered economical to mine and hence the only one in operation. Exploration has been difficult in this prospective province, due to a thick blanket of cover (e.g. Mesozoic sedimentary units) overlying the Cu-Au enriched Hiltaba granite basement (Lambert *et al.* 1987). Despite this challenge, the area still remains highly prospective with innovative exploration methods being implemented. One such technique involves investigating the regolith-landscape evolution for an area (Craig *et al.* 1999).

The opal mining town of Andamooka is located on the Stuart Shelf approximately 600 km north of Adelaide and 30 km east of Roxby Downs (Figure 1). Due to the prosperity of opal mining in the region and its proximity to Olympic Dam, further mineral exploration in Andamooka has been relatively incomplete. Research completed in the area has either been on a regional scale or has been concerned with the presence and distribution of opal (Johns 1968; Carr *et al.* 1979). Although these publications are focused on opal, they also provide an insight into the overall geology of the district. The following geological units have been proposed from the surface geology around Andamooka; – Proterozoic metasediments (Adelaidean) and granite (Hiltaba suite) basement underlying Neoproterozoic quartzite (Arcoona Quartzite), unconformably overlain by Cambrian limestone (Andamooka Limestone) which lies beneath a Mesozoic cover of sediments (Figure 2) (Wopfner *et al.* 1970; Carr *et al.* 1979; Lambert *et al.* 1987). The Mesozoic sediments preserve evidence of a transition from a terrestrial-fluvial environment (Algebuckina Sandstone) to a transgressional

marine setting (Cadna-owie Formation and Bulldog Shale) (Wopfner *et al.* 1970). This stratigraphy has been well documented with similar observations made over much of northern South Australia and western Queensland (Wopfner *et al.* 1970; Twidale and Campbell 1991; Campbell and Haig 1999; Veevers 2006; Wopfner 2010). It is widely accepted that the Mesozoic sediments, which cover much of the area, were deposited in a sedimentary basin (Eromanga Basin) that initiated in the early Jurassic, forming over the previously stable Gondwana surface (Wopfner 2010).

1.2.1 Algebuckina Sandstone

Stratigraphy

The term Algebuckina Sandstone was first used by Sprigg (1958) to classify “a gently dipping sequence of cross bedded grits and sandstones... which overlap on to the folded Precambrian of Mt. Dutton and the Peake and Denison Ranges”. This term has since been modified by Wopfner *et al.* (1970), to further classify the change within the stratigraphy. The Algebuckina Sandstone at Andamooka consists of medium grain to conglomerate arenite beds (occasional presence of gold), unconformably overlying pre-Jurassic rocks, which vary from deeply weathered and kaolinized material to quartzite. An upper and lower unit of the Algebuckina Sandstone has been defined (Wopfner *et al.* 1970) - the lower unit consists of moderately well sorted fine to medium grained kaolinitic sandstone, with angular to sub angular milky to clear quartz grains. Pyrite concretions and pebble conglomerate units appear mid-way through the unit with angular current bedding. The upper part of the unit is characterized by ferruginous layers leading to very well sorted clean semifriable quartz sandstone (quartz arenite), with silicification producing a quartzitic crust

(Figure 3). The unit is disconformably overlain, generally by the Cadna-owie Formation.

Other distinguishable features include the abundance of kaolinite and absence of feldspars, wood and leaf fossils preserved at the top of the unit, and preservation of angular and concavely current beds in the upper sandstone. Overall this unit has a high porosity factor, which has resulted in multiple stages of ferruginisation throughout beds in the upper part of the unit.

Depositional environment

Wide exposures of Algebuckina Sandstone have been noted along the south western margin of the Eromanga Basin around Oodnadatta (Algebuckina Hill), Mount Dutton and the Peake and Denison Ranges. Using observations made at sporadic exposures of the Algebuckina Sandstone, the following depositional interpretations have been made by Wopfner *et al.* (1970) and Harris (1962). Fossilized wood, fern and other plant fossils preserved in the upper well sorted sandstone have been defined as upper Jurassic to late Cretaceous age (Harris 1962). The environment at the time is described as terrestrial with a temperate climate (shown by the presence of ferns cycads and members of the *Araucariaceae* family (Harris 1962)). This indicates a fluvial terrestrial high weathering depositional environment for most, if not all, of the Algebuckina Sandstone's depositional history. The presence of large quartz and sandstone gravels at the base of the unit indicates a high energy fluvial system during the initial stages of deposition. As the sediments fine upwards, the energy of the environment is predicted to have subsided. This variety in sediment size, erosional features and the presence of angular and concavely current beds are all supportive of a braided river system.

Throughout and following the Algebuckina Sandstones's depositional history, the system is believed to have been subjected to intense weathering and erosion (Wopfner 1964). This is shown by the dominance of rounded quartz clasts, presence of alluvial gold and dominance of kaolinitic grains observed throughout the system.

Subsequently, the protolith was presumably rich in quartz and aluminium silicates, with the highly resistant quartz grains remaining relatively stable throughout the entirety of the depositional system. Meanwhile the aluminium silicates (presumably feldspars) are believed to have weathered to the kaolinitic matrix observed today. The effect of latter stages of erosion (during the Algebuckina Sandstone's depositional history) is also noted by the erosional disconformity of the overlying Cadna-owie Formation, which marks the onset of the marine transgression.

1.2.2 Cadna-owie Formation

Stratigraphy

The term Cadna-owie Formation was first proposed by Wopfner *et al.* (1970) to describe the mappable transition from the Algebuckina Sandstone to the Bulldog Shale. Wopfner *et al.* (1970) noted that despite the overall heterogeneity of the composition, the unit is clearly distinguishable by its "characteristic arenaceous rock types...and gently undulating erosion surface on the Algebuckina Sandstone". At Andamooka, the base of the Cadna-owie Formation is marked by an erosional disconformity overlying the Algebuckina Sandstone. The lower part of the unit is characterised by well sorted fine to medium grained sandstone, ranging to kaolinite in parts, distinguishable by buff-brown colour staining throughout (caused by weathering of the sandstone). This is overlain by ~2-5 m of prominent well cemented iron oxide sandstone (i.e. ferricrete), which also shows mottled staining observed in

the lower part of the unit. A white coloured fine sand layer with pyrite concretions is found in the upper middle section. This is followed by characteristic calcareous beds marking the upper part of the Cadna-owie Formation, capped by milky quartz clasts locally cemented in a highly resistant silicified matrix. This Cadna-owie Formation is conformably overlain by the Bulldog Shale (Figure 4).

Fossils have been observed throughout the Cadna-owie Formation (Harris 1962; Ludbrook 1965; Ludbrook 1966; Wopfner *et al.* 1970). Plant and fern fossils have been found in the lower Cadna-owie Formation, similar to those observed in the upper Algebuckina Sandstone. Fossilised microflora and limited fauna have also been documented, with *Gaudryinella permacra* the only diagnostic fossil indicating a marine environment (Harris 1962; Ludbrook 1966).

In other areas of exposed Cadna-owie Formation (such as at Mount Anna and Oodnadatta) the lithology varies, containing an abundance of mica and feldspar minerals that are importantly lacking in the overall Algebuckina Sandstone stratigraphy. Rhyolite pebbles observed at Mt Anna (classified as Mt Anna Sandstone Member) and interpreted as being sourced from the Gawler Range Volcanics, have considerable implications for the interpretation of the continental environment at the time of deposition (Rogers and Freeman 1993). The Mt Anna Sandstone Member was not observed in the study area.

Depositional environment

Until Wopfner *et al.* (1970) classified the Cadna-owie Formation (similar to the one defined above), the boundary between the Jurassic fluvial sandstone and the Cretaceous marine sediments was relatively undefined and consequently under-classified. In the majority of cases, where part fluvial to marine sediments were

observed it was largely either classified as Algebuckina Sandstone or Bulldog Shale, with some guesswork involved. Using the classification above, the following depositional setting can be interpreted. Prolonged periods of intense weathering and erosion resulted in a new depositional environment, overlying the previously formed Algebuckina Sandstones (evident by the undulating erosional surface). The base fine sand is believed to have formed in a marginal marine (beach) setting with well sorted fine sand grains being deposited. As the transgression gradually took place, the water level migrated over these sand beds, depositing calcium carbonate rich material (dead marine organisms), similar to that observed in present day shallow marine systems. As the sea transgressed further inland, the water depth increased, leading to the deposition of the Bulldog Shale. The mottled staining observed throughout patches of the unit occurred later as it was subjected to oxidation and intense weathering, in particular affecting the iron rich sediments in the stratigraphy.

The presence of feldspars and micas noted elsewhere in the Eromanga Basin provide a greater insight into the continental environment at the time. As both feldspar and mica minerals are significantly susceptible to weathering, a system allowing for rapid deposition is required. This consequently implies a mild tectonically unstable environment. The clasts of Rhyolite pebbles, found in the Mt Anna Sandstone Member (which are derived from the Gawler Range Volcanics) provides evidence for a direction of flow to be determined (Rogers and Freeman 1993). The stratigraphy sequence is believed to have formed in a high energy tectonically unstable environment with river systems originating in the west, and depositing sediment to the east (Rogers and Freeman 1993).

1.2.3 Bulldog Shale

Stratigraphy

The Bulldog Shale provides further evidence for an intracontinental marine transgression setting. The name Bulldog Shale has been used to describe the dominant marine sediments observed in the Eromanga Basin, consisting of a relatively homogenous lithology throughout the basin (Twidale and Campbell 1991; Campbell and Haig 1999; Veevers 2006). For this study the term Bulldog Shale will refer to the following (Carr *et al.* 1979) – overlying the top of the Cadna-owie Formation, an approximately 30cm thick conglomerate unit (known locally as bulldust) marks the base of the Bulldog Shale. The conglomerate contains rounded quartz to quartz arenite clasts ranging in sizes from 1-5 cm. This is conformably overlain by a fine grained carbonaceous, muddy to shale matrix (known locally as mud) with poorly sorted fine quartz grains and interbedded with a dark coloured ~3 cm thick member containing an abundance of pyrite and weathered pyrite concretions. This is overlain by a highly weathered, kaolinized and clay soil horizon (known locally as kopi) with large gypsum crystals forming downwards into the unit. Occasional patches of opal have been found to occur in the Bulldog Shale, commonly found between the kopi and mud subunits (Figure 5).

Fossils preserved throughout the Bulldog Shale, particularly in the carbonaceous unit include - crustaceans, ammonites (e.g. *Australiacera sjackii*), and bivalves (e.g. *Maccoyella barklyi*) (Day 1974).

Depositional environment

The presence of fossilised marine organisms provides a significant insight into the time and type of environmental setting for the Bulldog Shale. Crustaceans, ammonites and bivalves are all marine organisms with similar ancestry observed today. The environment would have therefore been similar to a shallow marine setting of today. These organisms thrived in the lower Cretaceous (Jablonski 1987), consequently an age can be defined for the sediments which preserve these fossils. Further work by Exon and Senior (1976), Senior *et al.* (1978), Veevers (2006) and Campbell and Haig (1999) has refined the Bulldog Shale age from Aptian to Albian (lower Cretaceous). Exon and Senior (1976) also noted similar marine sediments in neighbouring basins to the Eromanga (Carpentaria and Surat), concluding ~60% of Australia was submerged during the early Cretaceous.

Another feature of note in the Bulldog Shale is the quartz conglomerate unit which is believed to have been sourced from the underlying Cadna-owie and Algebuckina Formations. As the transgression was in the early stages, the energy of the overall system would have been relatively higher, similar to pebble lag horizons that form during the onset of marine transgressions (Bhattacharya 1993; Donovan 1993; Leithold 1994). As this subsided overtime, finer grained sediments (mud to shale) were deposited with carbonaceous members attributed to the greater presence of marine organisms.

Veevers (2006) speculates that the Bulldog Shale also contains an ash component in the matrix, which originates from volcanism relating to extensional activity during the breakup of the previously stable Gondwana supercontinent (Powell *et al.* 1988).

Veevers (2006) suggests that volcanism was occurring simultaneously with the

marine transgression on land, with emissions from the adjacent arcs settling into the newly formed ocean where it was deposited within the Bulldog Shale matrix. Such a conclusion leads to the following question of whether the marine transgression was triggered by this rifting or whether external factors were at play. Numerous authors have investigated this problem (Twidale and Campbell 1991; Campbell and Haig 1999; Veevers 2006), with many linking this transgressional event with a similar Cretaceous marine transgression preserved in Northern America's stratigraphy, the Western Interior Seaway (Hart and Plint 1993; Nummedal and Molenaar 1995; Campbell and Haig 1999). They argue that these two events imply globally high sea levels during the Cretaceous that inundated many continental areas including the previously stable Gondwana surface.

1.3 Regolith and landscape evolution

Andamooka is a dynamic evolving landscape, with continuous erosional processes shaping numerous landforms observed today. These erosional processes, in particular wind and water drainage, have produced a regolith dominated environment with limited exposed geology in the area. The word "regolith" is derived from the Greek words for blanket or cover (*regos*) and rock (*lithos*). The definition of what defines a regolith terrain has been fairly disputed in the past, with workers questioning whether regolith should be restricted to unconsolidated material (Jackson 1997) or include sequences of cemented units within unconsolidated units (Taylor and Eggleton 2001). As cemented layers (e.g. silicified conglomerates) were observed within the Mesozoic sediments and are still considered regolith components, this study will follow the definition of Taylor and Eggleton (2001) – "*Regolith* is all the continental lithospheric materials above fresh bedrock and including fresh rocks where these are interbedded

with or enclosed by unconsolidated or weathered rock materials. Regolith materials can be of any age”.

The region contains multiple colluvial erosional plains and rises, which constitute the majority of the landscape. The term colluvium refers to the mass deposition of material transported down a slope due to the influence of gravity and gravity influenced flow (e.g. drainage) (Taylor and Eggleton 2001). Colluvium deposits noticeably lack internal bedding structures and characteristically contain a wide range of grain shapes and sizes. The source for the sediments is generally derived from local hill tops where eroded material from rock exposures are moved down slope via hill creep, sheetwash and/or landslides. Two hills of significance to this project include Trig Bluff and Hill 1 (an unnamed hill adjacent to Blue Dam). As a consequence of their substantial elevation, these hills are continuously subjected to intense weathering and erosion. Weathering and erosion agents – wind, water and gravity – are predominantly responsible for lag transportation onto the plains below. These hills remain erect despite their significant exposure to weathering due to a silicified indurated duricrust at the top of the hills. These silcrete layers are extremely hard and highly resistant to erosion and can thus be subjected to higher weathering factors over sustained periods of time with less of an effect.

Another landform of note in the area includes the saline, Lake Torrens, located to the east of the Andamooka town centre. A main drainage depression is observed in the study area orientated in a north-west to south-east linear direction, flowing from the plains and rises into Lake Torrens. Despite being generally dry, flood plains and drainage scarps are observed immediately adjacent to the lakes boundaries. These

contain an abundance of clay and sand sediments (with minimal lag) layered during ephemeral wet periods.

1.4 Remote sensing background

Remote sensing is the use of sensors at a distance to acquire and analyse information. A modern practice of remote sensing is the use of spacecraft and airborne sensors to measure transmitted and reflected electromagnetic radiation from the earth's surface. Reflective values received by the sensors are then used in a wide range of analyses for interpretation of features on the earth's surface. This study evaluates the ability of using Advanced Spaceborne Thermal Emission and Reflection Radiometer (ASTER) on board the Terra satellite for geological and regolith-landform mapping around the Andamooka area.

The ASTER sensor is a joint venture between Japan (METI) and America (NASA) and was designed to produce high resolution multispectral images for interpretations of surface temperature, elevation, reflectance and emissivity. The ASTER sensor contains 15 bands with measurements in the visible-near infrared radiation (VNIR), shortwave infrared radiation (SWIR) and thermal infrared radiation (TIR) (Figure 6). ASTER contains a backward scanning band labelled VNIR_band3B designed to calculate and produce digital elevation models for the mosaic tiles (Kalinowski and Oliver 2004). It is important to note that this band should not be used in the interpretation and processing of images, and thus should be excluded. The remaining 14 bands can be used in combination with each other to enhance and mask absorption features in the respective parts of the spectrum (Kalinowski and Oliver 2004).

2. Methods

To meet the project aims of constructing a regolith landform map, interpreting the landscape, and assessing the accuracy of using remotely sensed data, a combination of field observations and laboratory work was performed. This section describes the processes and steps completed to achieve these aims.

2.1 Regolith-landform mapping

Regolith-landform mapping encompasses the representation of regolith materials, incorporating both the geomorphology and landscape controls for the individual regolith landform units (RLUs) (Taylor and Eggleton 2001). It is of particular use for areas where rock outcrop exposures are limited, and minimal previous geological knowledge is known. Observations taken in the field included sediment orientation, mineralogy, colour, consistency, porosity, rock strength, fabric, geomorphic processes, grain size, sorting, lag, landforms, and weathering degree, processes and structures. This classification follows guidelines suggested by Pain (2008). RLUs are based on a combination of regolith units and their associated landforms, employing a code system as shown in Figure 7. Units were characterised and classified based on this system whilst in the field. GPS coordinates, and vegetation types were additionally recorded. Grab samples were also collected at designated spots to represent the soil and lag of each RLU (Figure 8). These grab samples were then used for a range of analyses, including examination under the PIRSA (Primary Industries and Resources South Australia) Hylogger, and a series of diagnostic soil tests (exact methods used in these tests are described in the following subchapters). This data

aided in the production of the regolith landform map by helping to classify the RLUs. The map was digitised based on the combined data from the RLUs (aided by corresponding GPS points), with polygons digitised over georegistered background aerial imagery and geology maps in ArcMap.

2.2 Soil diagnostic tests

Diagnostic tests were performed on the soil samples to analyse unique properties of the soil. These tests included determining the texture, structure, colour and pH of the soil. Soil texture is a measure of consistency, sampled using a small handful of soil to represent the unit as a whole. The consistency is measured by kneading a handful of moistened soil (approximately at field capacity) into a ball and ribboning the ball between the thumb and forefinger. Textures are determined based on the feel of kneading the soil and the length of ribbon achieved. The ribboning length is a good indicator of the particles within the soil. Generally, shorter ribbons indicate greater sand content, whilst longer ribbons indicate greater clay content. Wetherby's (2006) soil classification chart was used as a guideline to classifying soil textures (Figure 9). Soil colour was also determined at field capacity. Colour values were determined using the standard Munsell Colour Chart to approximate the hue, value and chroma of the soil i.e. 10 YR (hue) 5 (value) / 2 (chroma). Apart from giving the reader an interpretation on the soil's appearance, colour values can be an indication of a soil's drainage property. Reddish hue's within a B horizon indicate a high porosity, well drained soil, whilst yellowish hues and gleys indicate poor drainage (Wetherby 2006). Soil pH is a measure of acidity or alkalinity within the soil. It is an important property of soils, as the pH has significant controls and consequences on chemical processes. An example of such is the presence of extremely high acidic soils around oxidized

pyrite. The pH was tested by placing small amounts of the soil samples on a spot plate and mixing them with dye indicator to their saturation point. Barium sulphate was then sprinkled on top and left to rest until a change in colour was noted. The change in colour was then compared with a pH colour card to approximate the pH of the soil (accuracy ± 0.5). These soil diagnostic tests were then combined with field observations including lag, landforms, vegetation and GPS coordinates to help classify similar RLUs.

2.3 Hylogger analysis

Surface samples collected in the field at differing RLUs were separated into soil and lag components in preparation for analysis with PIRSA's Hylogger. The Hylogger uses automated core tray handling, continuous visible and infrared spectroscopy and digital imaging to characterise and identify spectral signatures for the mineralogy (Mauger *et al.* 2004). These spectral signatures show absorption features within measured spectral ranges characteristic of the mineral. For example, kaolinite is distinguishable from other clay minerals by a doublet absorption in the 2200 nm range (Mahoney *et al.* 2002) (Figure 10). Preparation of samples included placing approximately 200 grams of each soil sample within labelled rock chip trays. Lag samples were placed within labelled clear bags with at least one sample of each different lag unit observed at each site. As the Hylogger is primarily used for scanning standard sized core trays, the range and scope of the Hylogger sensor had to be adjusted for the lag samples. To represent the lag observed on the surface, the whole rocks from each profile were placed on the conveyor belt in a line of approximately 70 cm to 1 m. The Hylogger takes a photo of each sample and then scans horizontally across the profile, propagating down with each completed scan. This resulted in a

series of spectral signatures for the samples, which were analysed and processed by Georgina Gordon, a specialist spectral geologist with PIRSA. Processed data was in the form of TSG files, viewed in TSG Viewer¹. These files include images of the samples and their associated main minerals as predicted by the software, based on their SWIR and VNIR signatures. This information was used to help distinguish RLUs based on their mineralogies.

2.4 ASTER analysis using band ratio processing

The ASTER sensor is an improvement on the previously launched Landsat instrument. It records an extra seven bands of the electromagnetic spectrum, with more coverage over the TIR (Kalinowski and Oliver 2004). These extra values allow for greater geological spectral analysis, such as distinguishing between Al-OH and Mg-OH groups. However, the ASTER sensor (a multispectral instrument) does not provide the same coverage as more expensive hyperspectral imagery e.g. HyMap. Consequently, ASTER bands can only predict abundances of mineral groups, rather than specific minerals.

Band ratios and relative absorption-band depth (RABD) ratios have been shown to be a successful tool in distinguishing mineral groups, to aid in the production of regolith mapping (Crowley *et al.* 1989; Mah 2002; Hewson *et al.* 2002; Rowan and Mars 2003). Recognized successful band ratios from ASTER data were used to highlight key mineral groups and landforms within the mapping area (Table 1). Band ratio imaging uses measured values from the individual spectral bands (measured by the

¹ “TSG Viewer is a free version of TSG which allows users to view already processed TSG files from both TSG Pro and TSG Core. It has been designed for users who do not want to carry out any processing, but who wish to be able to view and plot already processed spectral data for report writing, or for sharing results with other colleagues.” http://www.thespectralgeologist.com/tsg_viewer.htm.

ASTER sensor) to highlight significant absorption and reflectance features. This is achieved by running a model which divides one band's strong absorption signal by another band's weaker signal (e.g. band 5/band 6). RABD ratio imaging uses the addition of multiple bands which border strong absorption features and divide that value by a band which records minimal absorption (i.e. $RABD = (Band\ X + Band\ Y)/Band\ Z$). However before processing of the ASTER band ratios can be conducted, images must be pre-processed.

ERDAS Imagine software was used in the production of pre-processed and processed ASTER imagery. The ASTER sensor measures reflectance values over 3 parts of the spectrum VNIR, SWIR and TIR. Consequently raw ASTER images are separated into subsets of these three parts of the spectrum (with an extra image in the VNIR used in the calibration of elevation values). A layer stack was conducted to incorporate all 14 bands into one useable image. This file was then reprojected to GDA94 Zone 53 to align with GPS coordinates taken in the field. Additionally, the image was clipped to only incorporate the project area to help with a supervised classification and accuracy assessment i.e. ground truthing. Despite ASTER bands measuring within atmospheric windows, distortion was still noted in the imagery and thus had to be accounted for before use. A log residual tool was consequently used to atmospherically correct the data to pseudo-reflectance (DN values). A log residual tool divides each pixel's reflectance value (R_{pv}) by the band's mean (R_{bm}) and the mean of the whole image (R_{mi}) (i.e. $\log\ residual\ DN\ value = R_{pv} / R_{bm} / R_{mi}$). This quick atmospheric correction tool accounts for atmospheric absorption, solar illumination and sensor gains. Notably cloud coverage is not corrected by this algorithm and had to be acknowledged in any processed imagery. The log residual image was considered a viable representation of the surface geology and used in the production of band ratio images. The model

maker tool enabled the selection of band ratios (Table 1) to enhance spectral responses of interest. Resulting images were then used in conjunction with the georegistered regolith map to firstly assess the validity of using ASTER data for the project area and secondly highlight any features of interest previously overlooked.

2.5 Supervised classification using combined ASTER data and field observations

A supervised classification was conducted in ERDAS Imagine using sample location points as training areas. Area of interest (AOI) rectangles were digitized around GPS coordinates of known units found in the field (e.g. Trig Bluff, opal diggings, Hill 1, plains consisting of Bulldog Shale (CHep₂) etc.). Multiple AOI rectangles were selected as training sites, to represent the average spectral signature of the individual units. A minimum distance to means classifier was then performed. This associates pixels in the image to the nearest training signature.

2.6 Digital elevation model

A digital elevation model was obtained from the Shuttle Radar Topography Mission (SRTM) acquired in 2000 (Rabus *et al.* 2003). A standard deviation stretch was performed in ArcMap to show enhanced visually identifiable elevation values for the project area.

3. Results

Field observations are an integral component for understanding landscape features and provide vital information to predict how the landscape evolved. It is important to understand where units lie in the overall context of the system, such that anomalous areas stand out for further investigation. In this study, field observations have contributed significantly to interpretations made on the landscape evolution. Soil diagnostic tests and remote sensing data were used to further examine areas of interest noted in the field.

3.1 Regolith-landforms

The regolith landform map is shown in Figure 11. Soil diagnostic tests further enhanced the classification of the regolith units (Appendix 1). The map contains information that was important in the overall landscape evolution interpretations made for the area. This section will discuss the key regolith landforms classified within the mapping area, describing the colluvium, aeolian and alluvial sediments observed (for a full list of RLUs classified in the project area, see Table 2).

Colluvium erosional plains, hills and rises

The majority of the landscape in the study area is comprised of colluvial erosional plains dominated by poorly sorted angular lag. The colluvial plains occur primarily at two elevations, with higher elevated plains to the west relative to the east.

Significantly, the plain classified as CHep₂ (Figure 11) appears at both elevation levels. CHep₂ was classified based as a sheet flow erosional plain distant from sand dunes. The soil contained an abundance of clay and loam particles with a greater soil

structure noted than adjacent plains. Lag included sub-angular to rounded iron stained quartzite (1-20 cm), abundance of rounded and angular yellow/red silcrete (commonly known as jasper, 2-10 cm), thinly layered flat quartzite (5-10 cm), rounded fluvial pebbles, patch opal, cemented kaolinite pebbles and small rounded hematite and goethite nodules. Vegetation included saltbush (*Atriplex* and *Rhagodia* spp.), long-spined bindyi (*Sclerolaena longicuspis*) and grasses. This unit comprises part of the Bulldog Shale, as exposures indicative of Bulldog Shale were noted adjacent to these two plains within drainage depressions. Opal diggings occur within the higher elevated CHep₂ plains, with occasional abandoned opal digging also noted in the lower CHep₂. These plains are separated by sheet flow erosional rises grouped as CHer₂. CHer₂ contains a similar lag and soil component to that observed on CHep₂. The lower slopes of the rise contain patches of exposed Cadna-owie Formation (beach sands) with areas of more ferruginous content. The upper slopes are marked by the appearance of pyrite and carbonates with fine clay and mud sediments indicative of the Bulldog Shale formation. Bulldog Shale was observed at the top and bottom of these rises, with the Cadna-owie Formation present in between. Similar disconformities were noted within the landscape setting at hills Trig Bluff (Ceh₁) and Hill 1 (Cel₂). Trig Bluff consists of Algebuckina Sandstone along adjacent slopes, with the lower unit consisting of moderately well sorted fine to medium grained kaolinitic sandstone, with angular to sub angular milky to clear quartz grains. Pyrite concretions and pebble conglomerate units appear mid way through the formation with angular current bedding. The upper part of the unit is characterized by ferruginous layers leading to very well sorted clean semifriable quartz sandstone (quartz arenite), with silicification producing a quartzitic crust resistant to weathering.

The hill is surrounded by older sheet flow plains (CHep₅) dominated by flat angular quartzite lag characteristic of the Arcoona Quartzite.

Exposures of Arcoona Quartzite were found within CHep₅, with flat horizontal beds of massive quartzite observed *in-situ* (Figure 12). Steeply bedded angular sheared outcrop exposures were found in a strongly linear NE-SW orientation approximately 500 m from these exposures (Figure 13). Patches of gypsum and kaolinite soils (Figure 14) were found in close proximity to these shear zones. Additionally, iron rich fluid flows (forming along joints) and manganese staining were observed immediately adjacent to these shear zone.

Hill 1 contains multiple exposures of the Cadna-owie Formation, observed within drainage depressions down slope of the hill crest (eastern side). Exposures include well sorted sandstones and kaolinite at the bottom, ferricrete, carbonaceous and pyrite concretions appearing in the middle units, and silicified conglomerates capping the top. Immediately below the hill in the drainage depression, adjacent to Blue Dam, is exposures of Bulldog Shale. This provides a further example of younger stratigraphy (Bulldog Shale) underlying an older formation (Cadna-owie Formation).

Aeolian sediments

Aeolian sediments, such as sand dunes, cover a majority of the interior Australian continent (Wopfner and Twidale 1967). Of significance to this project include longitudinal sand dunes located in the north and west of the project area. Longitudinal sand dunes require a change in wind direction to allow for their linear orientation (Wopfner and Twidale 1967). As the sand dunes contain a relatively homogenous composition and distribution, they are hereby classified into two groups ISul₁ and ISul₂. ISul₁ are sand dunes located in the west of the mapping area adjacent to CHep₁.

The unit consists of aeolian deposited quartz sands with an iron component. ISul₂ is classified as longitudinal sand dunes located in the north of the mapping area. These dunes contain a carbonate influence (observed by patches of white calcrete within the soil) due to the presence of underlying limestone. Both units are clearly distinguishable on the ASTER band ratio imagery.

Alluvial sediments

Lake Torrens (Lpl₁) is a dry endorheic rift saline basin that formed within the Torrens Hinge Zone (Twidale 1972; Belperio and Flint 1993). Many drainage depressions are observed in the study area orientated in a north west to south east linear direction.

Despite being generally dry, floodplains and drainage scarps are observed immediately adjacent to the lakes boundaries. These contain an abundance of layered clay and sand sediments (with little lag) which formed during significant wet periods. Apart from providing patches of exposed geology, which aid in the interpretation of the landscape, the depressions remain relatively uniform. Consequently, the majority of depressions have herby been classified as Aed₁. These depressions include, an abundance of reworked rounded sediments from the upper plains, including quartzite pebbles, pink shales and conglomerates. An abundance of kaolinite and lack of sand within the poorly structured soils along drainage beds was also noted. These depressions are easily identifiable in the field and on remote sensing imagery due to the abundance of vegetation in a linear orientation. Vegetation includes high density Bullock Bush (*Alectryon aleifolius*), Western Myall (*Acacia papyrocarpa*), bluebush (*Maireana* spp.), grasses, *Malva* sp. and saltbush (*Atriplex* and *Rhagodia* spp.).

3.2 Remote sensing imagery

Digital elevation model (DEM)

Field observations found the distribution of opals confined to the higher elevated plains consisting of Bulldog Shale (CHep₂). A correlation between the distribution of opal diggings and elevation was conducted to quantify this field observation. A statistical t-test was conducted for the opal diggings within the digital elevation model (Appendix 2). The opal diggings were found to occur at an average elevation of 107.6 m above sea level, significantly higher than the surrounding study area (mean = 81.5 m; P-value < 0.0001; df = 248). The DEM also highlights drainage patterns mirrored in the regolith-landform map. The drainage depressions in the study area are concentrated where the elevation gradient is highest (i.e. in between high and low elevation areas). In addition to the general northwest to southeast drainage pattern, smaller offshoot drainage depressions from south west to north east are also identifiable.

Band ratios of ASTER

Recognized ASTER band ratios (Hewson *et al.* 2002; Mah 2002) and relative absorption band depth ratios (Table 1) (Ninomiya and Fu 2001; Crowley *et al.* 1989) were used to compile ASTER imagery (Appendix 3). These assisted in the production of the regolith-landform map. Any cloud coverage within the imagery causes high reflectivity over most bands, and has consequently been noted for exclusion in Appendix 3. The ASTER CSIRO regolith ratios were particularly useful in distinguishing sand dunes, showing high contrast between the iron oxide rich sand

dunes (shown in red) and the clay rich plains (shown in blue) (Appendix 3). Drainage depressions are distinguishable as thin pink stripes, with a prominent drainage depression orientated NW-SE terminating at Lake Torrens. Smaller drainage depressions are connected to this main depression. The smaller depressions are approximately orientated in a SW-NE orientation. Opal diggings appear as distinct white pixels bordered by light blue pixels. The upper slopes of CHer₂ are also represented by these light blue pixels, with CHep₂ (plains consisting of Bulldog Shale) identifiable by its strong red/purple pixel colours.

The clay amphibole and laterite (CAL) band ratio image highlights similarity in the mineralogy between the upper and lower CHep₂ plains. It shows an assortment of pixel colours, representing the combination of lag and soil components observed in these plains. These pixels strongly contrast the adjacent plains which are dominated by a clear pink and blue colour, indicating the homogeneous composition of the Andamooka Limestone, Arcoona Quartzite and lacustrine plains (SMep, CHep₅ and CHpl₁). Drainage depressions are also clearly distinguishable (Aed₁).

The silica, carbonate and basic (SCB) band ratio image and the carbonate clay and siliceous (CCS) band ratio image both contain an abundance of noise. This is evident by the lines of distortion in their resulting images causing a blurred affect. The noise is caused by the use of the TIR band 14 in the classification of carbonate groups. This band has been known to receive crosstalk from the adjacent bands and thus any carbonate classifications should be used with scepticism. The CCS image superiorly reflects the Andamooka Limestone as red pixels compared to the SCB image. Additionally, the CCS image strongly represents the opal diggings as homogeneous green pixels i.e. clay.

Similarly, the structural features (SF) band ratio shows the opal diggings as bright blue pixels. The SF image also shows linearly orientated thin structures, vaguely represented by thin bands of blue-green pixels. In most cases these bands appear immediately adjacent to drainage depressions, but they also appear on the plains.

The Al-OH band ratio image clearly distinguishes boundaries between differing landforms. In particular the image represents the wash off of slopes that forms the smaller drainage depressions, displaying these areas as white-light pale blue pixels. This image strongly reflects the drainage contours of that perceived in the DEM and that of the RLU boundaries between CHep₅ and CHer₃.

The band ratio image highlighting areas of discrimination for mapping was particularly useful in distinguishing the boundary between CHep₁ and CHep₂. CHep₁ is clearly distinguishable by its vibrant yellow colour pixels similarly reflected in the brighter colour pixels observed for the sand dunes.

Supervised classification

The supervised classification (Appendix 4) is limited to the amount of knowledge known for the area. Pixels were associated to training sites based on their signature values, which best reflected the training sites spectrum average. Consequently, pixels could only be associated to predefined classes, which is not ideal for heterogeneous landscapes. Despite multiple misclassifications being noted (e.g. opal diggings as clouds), the supervised classification remarkably reflects the base of the CHer₂ RLU. The pixels labelled as Cadna-owie Formation in the supervised classification largely mirror those identified in the RLU as CHer₂. Furthermore, the boundary with the Bulldog Shale in the upper slopes of the unit is also shown. As such, this technique

provides a possible way of distinguishing the approximate boundary between the Bulldog Shale and the Cadna-owie Formation.

3.3 Hylogger analysis

Appendix 5 lists the main minerals predicted for the lag and soil samples based on their SWIR and VNIR spectral signatures. From the SWIR signatures the Hylogger primarily seems to be able to predict and distinguish between clays and other Al-OH minerals. This is evident by the mineral abundances predicted in the samples, the most common minerals including, kaolinite, montmorillonite, muscovite, illitic-muscovite, dickite and palygorskite. In addition the Hylogger is also able to successfully determine the presence of carbonate minerals with calcite, dolomite, ankerite and siderite all being associated with units known to contain a carbonaceous component (i.e. Andamooka Limestone SMep, Bulldog Shale CHep₂ and upper part of the Cadna-owie Formation CHer₂). The VNIR signatures from the Hylogger were able to distinguish the presence of Fe-O minerals - goethite and haematite. In the majority of cases goethite was associated with aspectral minerals. Noticeably quartz and siliceous minerals were significantly under classified. Despite numerous silcrete and quartzite lag samples being analysed, no Hylogger results indicated siliceous minerals. Commonly these samples were classified as aspectral or null, with occasional clay minerals (from weathered/and or contaminated soil/dust coatings) appearing in the results.

4. Discussion

Data analysis has been used to complement and contribute to field observations and interpretations for the landscape evolution. Mainly, field observations and data analysis have been used in combination to produce a regolith-landform map, which highlights details unattainable solely from the previous geological map for Andamooka (Figure 2). In particular, the Cadna-owie Formation and Algebuckina Sandstone lithologies have hereby been distinguished as separate units (previously grouped together). Additionally, surface disconformities have been investigated in detail, examining the boundaries between differing lithologies and the possible structures that could cause them.

4.1 Regolith-landform map and landscape evolution

The regolith-landform map visually conveys field observations made distinguishing lithological boundaries. These boundaries have significant implications for the proposed landscape evolution of Andamooka. Of particular significance, includes the observed continuous transitional boundary between the Cadna-owie Formation and Bulldog Shale made along the rises ($CHer_2$) of adjoining plains ($CHep_2$).

Additionally, Bulldog Shale exposures were noted beneath the Cadna-owie Formation (Cel_2) in adjacent drainage depressions. These observations consequently lead to the following interpreted stratigraphy of older (Late Jurassic-Early Cretaceous) Cadna-owie Formation interbedded between younger (Cretaceous) Bulldog Shale. As there is an obvious disconformity between these units, a structural input is required.

Extensional faulting is one mechanism proposed for this disconformity. Multiple

normal faults orientated in a NE-SW direction are predicted throughout the project area, resulting in sharp boundaries between differing units (Figure 15). In the majority of cases, these faults have not been directly observed due to overprinting of drainage depression sediments. However, a shear zone in a NE-SW direction was noted in the Arcoona Quartzite bordering the lower Bulldog Shale plain. This shear zone was distinguished based on observations of linearly orientated steep angular bedded outcrop exposures of Arcoona Quartzite, adjacent to a horizontally bedded outcrop. The Arcoona Quartzite widely remains homogenous with flat horizontal beds observed throughout the majority of the unit. The reduction in grain size also noted is interpreted as a mylonite texture, providing further evidence of shearing.

As the shear zone influences both the Arcoona Quartzite and Bulldog Shale, an approximate age can hereby be defined for this extensional stress. Extensional forces must have been present from as young as the Cretaceous. As the Australian continent has not been on a plate boundary since the Cretaceous, intracontinental stresses presumably play a vital role in faulting for this area (Sandiford 2003). However, the shear zone itself may have originated as late as the Neoproterozoic, with younger reactivated faults possible. The landscape evolution is hence predicted to have been significantly controlled by tectonic activity in the area. Extensional faulting may account for the distribution of Bulldog Shale (CHep₂) at high and low elevations, with outcrop hills of Cadna-owie Formation and Algebuckina Sandstone being exhumed. Remnants of these hills are still exposed due to localised silicification producing a highly resistant indurated crust. These hills are hereby viewed as preserved horsts with the adjacent lower plains assumed to be grabens. Figure 16 illustrates the interpreted boundaries of the units with relation to predicted normal faults in the study area.

The presence of white kaolinitic and gypsum rich soils could be a direct result of faulting in the area. These soils were commonly found adjacent to these linear shear zones overlying Arcoona Quartzite. As this unit is pure quartzite and does not contain feldspar, the parent material for the kaolinite has previously been unknown (Wopfner 2010). It is proposed that these soils may have formed from transported material from the Bulldog Shale due to the abrupt proximity of these units, caused by the faults.

Alternatively, these soils may be remnants of the previously highly weathered Gondwana surface, discussed by Wopfner (2010).

Based on the geology, regolith-landform maps and band ratio images, there is an obvious contact boundary between the geology north and south of the main drainage depression. The main drainage depression in the north of the project area, orientated north-west to south-east, is also assumed to be overprinting a fault scarp. The DEM shows the contrast in elevation between the areas adjacent to this depression. An oblique dextral strike slip fault is assumed, allowing for the exhumation of the Cambrian Andamooka Limestone, whilst also accounting for the lateral displacement of the Bulldog Shale. The smaller extensional faults are believed to be connected to this larger strike slip faults i.e. an extensional duplex system.

Extensional faults caused by intracontinental neotectonism have also been documented in similar Mesozoic sediments elsewhere in South Australia (e.g. near Lake Eyre and Four Mile) (Reynolds *et al.* 2003; Sandiford 2003; Waclawik 2006; Hill and Hore 2010). Reynolds *et al.* (2003) attributes changing plate boundary interaction rates between the Indo-Australian and Pacific plates as the cause for intracontinental stress, resulting in these faults. Sandiford (2003) acknowledges the variation of stresses caused by modern plate boundaries as the possible mechanisms

for reactivation of faults for extensional activity across south-eastern Australia. Consequently, post Cretaceous extensional faulting allowing for the modern landscape formation is plausible.

Opal formation and distribution

Previous studies (Johns 1968; Carr *et al.* 1979) have discussed the stratigraphy of known opalisation and its presence in the Bulldog Shale. However, no studies have provided an overall model for opal exploration. The results presented above demonstrate, a strong correlation between successful opal diggings and regions of higher elevations, as shown in the DEM (Appendix 2). As the majority of diggings in the lower plains of Bulldog Shale have been unsuccessful, horst blocks caused by faulting are considered to be associated to opal distributions. One possible explanation for this is the oxidation of pyrite within the Bulldog Shale initiating opal formation. This proposed extensional faulting resulted in exhumation and oxidation of the pyrite rich lithology in the Bulldog Shale. Oxidation of pyrite resulted in the formation of sulphuric acid solutions that permeated throughout the Bulldog Shale leaching aluminium (Al) from aluminium silicates (such as kaolinite, shale etc.) from within the unit, leaving free silica. Opal then formed when the silica was hydrated (accumulated in the ground water), and precipitated due to fluctuating water table height within suitable crevices or trapped by permeability barriers.

This interpretation supports Carr *et al.*'s (1979) documentation of opal diggers' observations that opal is commonly associated with the up-thrown side of "slides" or "slips" (i.e. faults), often forming shallow flexure basins on the up-thrown side (Figure 5).

The pH readings taken from the plains consisting of Bulldog Shale were expected to show acidic values for these soils, however few showed significant results. This may be due to insufficient samples, pH re-neutralisation over time, unreliable results from surface soil or a fault with the field pH testing kit. Therefore soil pH findings can consequently not be solely used to prove or disprove this theory.

It should be noted that opal distributions have been largely based on aerial photography of successful opal diggings. The assumption that opal distribution is restricted to these diggings should be viewed with caution. For example it is possible that the opals are present within the grabens, however they have yet to be discovered due to the increased overburden.

Silcrete, jasper, goethite and haematite formation and distribution

Similar to the opal formation, exhumation and oxidation caused by extensional faulting is believed to have contributed significantly to the formation of siliceous and ferruginous materials in the region. Silcretes can broadly be classified into two groups – pedogenic and groundwater silicates. This study proposes that the majority of silcretes observed in the area are classified as groundwater silicates. These silcretes presumably formed at the palaeo-water table, post Cretaceous faulting. As the silica rich groundwater table height varied and percolated throughout the unit silica was precipitated and cemented around surrounding material, forming these silcretes. There is no evidence to constrain this silcrete formation to one period in the landscape evolution, but may have occurred during multiple fluctuations in the palaeo-water table. This model for silcrete formation is not solely restricted for the Bulldog Shale. The pyrite rich upper units of the Cadna-owie Formation and Algebuckina Sandstone

are assumed to have enabled the formation of localised silcrete, as observed on Trig Bluff and Hill 1.

Iron concentrations are believed to have formed synchronously with these silcretes.

As the pyrite oxidised, sulphur was stripped from the pyrite leaving high concentrations of iron accumulating in the soil and groundwater. Some of this iron accumulation is predicted to have bonded to the free silica in the groundwater contributing to the formation of jasper. Jasper is predominantly a chert distinguishable by its red to yellow colour, caused by iron inclusions in its composition. The abundance of jasper lag observed on the plains consisting of Bulldog Shale and adjacent landforms is the basis for this interpretation.

Iron nodules were also identified within equivalent plains of the Bulldog Shale. The presence of hydrated silica (opal) and iron oxide minerals (haematite and goethite nodules) further indicates an independent source of iron and silica relative to the parent jasper material. The presence of copious goethite in relation to haematite further suggests a hydraulic influence on the iron rich mineral's formation, with free water readily available. Iron rich groundwater solution is also believed to have contributed to ferricrete members observed in the topographically lower underlying units, the Cadna-owie Formation and Algebuckina Sandstone. This interpretation is based on the presence of iron rich veins percolating downwards within the Bulldog Shale profile (Figure 17). Although the Bulldog Shale contains a low porosity factor, the iron rich fluids are predicted to have propagated along fractures and faults within the unit, precipitating at oxidised redox boundaries i.e. within the Cadna-owie Formation and Algebuckina Sandstone. These units were then presumably subjected to multiple stages of ferruginization as a consequence of their high porosity factor.

4.2 ASTER analysis

Processed ASTER imagery was useful in distinguishing seemingly homogenous landform features with high reflectivity values, such as opal diggings, sand dunes, drainage depressions and Lake Torrens. In particular, ASTER band ratio images highlighting clay mineral groups (CSIRO regolith ratios, CAL, CCS) were assessed to successfully highlight opal digging boundaries. This is believed to be caused by opal diggings generally focused around the clay rich kopi layer. Consequently, surface material has been removed from these areas, leaving a homogenous clay layer exposed at the surface. Boundaries of opal diggings are also highlighted by contrasting colours, caused by waste from overburden discarded proximal to the diggings. The Al-OH image further classifies the clay minerals predicted for the opal diggings associating blue pixel values i.e. indicating a high probably of kaolinite. As field observations describe the abundance of kaolinite in the kopi layer, this band ratio image is assessed successful for identifying opal diggings. This further shows the accuracy of using ASTER band imaging (especially high reflectance values) for particular landforms.

The CSIRO Regolith ratio image was particularly useful in representing the plains of Bulldog Shale (CHep₂) and Cadna-owie Formation rises (CHer₂). These were distinguished based on assimilated red, blue and purple pixels, caused by the presence of clays and ferruginous minerals which dominate these units. This image allowed for the recognition of Bulldog Shale exposure on the northern side of the main drainage depression running northwest to southeast. As this site was not visited in the field, it was originally grouped as Andamooka Limestone. This was revised based on the CSIRO band image, displaying an anomalous pixel value which distinctly reflected

the southerly plains. This was further verified, with the previous geology map identifying the unit as a Bulldog Shale hill (locally referred to as Bill's Lookout). A dextral displacement component was hereby attributed to the fault exhuming the Andamooka Limestone, whilst laterally displacing the Bulldog Shale.

The enhanced structural image possibly represents the predicted fault scarps for the area. Thin green pixel groups were noted adjacent to drainage depressions, predicted to show outlines of the faults. Accuracy assessment is inconclusive due to the observed fault scarp within the Arcoona Quartzite being overshadowed by cloud cover in the area.

The band ratio image highlighting areas of discrimination for mapping strongly displays the longitudinal sand dunes (as yellow pixels) mapped in the north and west of the study area. Consequently, predictions can be made from the data, assuming the yellow pixels are a representation of the siliceous sand content. Resultantly, the plains adjacent to these sand dunes clearly show a strong sand component to their soils. As this was the distinguishing feature in classifying units CHep₁ and CHep₂, this image consequently shows the approximate boundary between these two differing RLUs.

Although processed ASTER imagery cannot solely replace field observations to conduct regolith-landform mapping, it has been shown to complement and highlight areas of significance in regolith dominated landscapes. In particular, homogenous and high reflective units were found to be reliably classified in several band combinations, further supporting field observations and interpretations.

4.3 Hylogger interpretations

The Hylogger data shows further evidence for association between the siliceous and ferruginous materials. Although siliceous minerals are not directly identified by the Hylogger system, it is assumed the majority of aspectral predicted materials are essentially siliceous. Due to the crystal lattice of the bonded silica to oxygen elements there is little to no absorption between interacting electromagnetic waves. Hence, as the spectral signatures do not have any diagnostic absorption readings (compared to most clay minerals), the siliceous minerals are classified as aspectral. Using this assumption it is evident there is a strong correlation between predicted goethite and aspectral/siliceous minerals from the Hylogger analysis. This supports the earlier assumption that silcretes were forming from siliceous groundwater, also highly concentrated in iron. Additionally, goethite and aspectral readings were not mutually restricted. Goethite and in some cases haematite were found to occur independently in lag samples, which were previously described as iron nodules.

4.4 Mineral prospectivity

Although Andamooka is renowned for prosperous opal mining, this study has found potential for further economic mineralisation in the area. The understanding of neotectonic activity, which is believed to have contributed significantly to the landscape evolution, potentially is the key to further mineralisation discoveries. Multiple iron rich (haematite) occurrences observed adjacent to shear zones in the area provide evidence of iron rich fluid mobility along shear zones. Coupled with numerous REDOX boundaries observed within the Mesozoic sediments, the area not only remains highly prospective for mineralisation mobility but also for trapping and

precipitating mobile fluids. The permeability difference between the porous Algebuckina Sandstone and Cadna-owie Formation and the impermeable Bulldog Shale further enhances the potential for secondary mineralisation in the Mesozoic sediments. Additionally, the presence of Olympic Dam (only approximately 20 km west) indicates a potential source of IOCG type mineralisation within the region (Olympic IOCG Province). Consequently, a source, transport mechanism (along the faults) and potential trap for mineralisation can all be found proximal to Andamooka. A similar exploration model previously implemented near Arkaroola was successful in identifying economic uranium mineralisation at Honeymoon and Four Mile (Hill and Hore 2010). High uranium concentrations were found to be hosted within the Eyre Formation and Bulldog Shale units, with secondary mineralisation at Four Mile constrained to grabens along extensional faults, similar to that observed in this study.

4.5 Scope for further study

For this project, it was widely assumed that the boundaries of extensional faults in the area have been overprinted by transported alluvial sediments. Consequently, few fault scarps were actually observed in the project area. Further geophysical studies could therefore be concentrated on proving the presence and distribution of the proposed extensional faults. One such study could be further use of the new high-resolution resistivity instrument developed by ZZ Resistivity Imaging Pty Ltd. This instrument has previously been used in the Andamooka Precious Stone Field, with test sites near White Dam investigating the use of this instrument to enhance opal exploration (Morris and Zhe 2010). These early trials have already proven to be a successful tool in delineating sub-surface fault structures, and correlating resistivity values with differing lithologies (Morris and Zhe 2010). Additionally, X-ray fluorescence (XRF)

readings could be measured around the observed shear zone bordering the Arcoona Quartzite and Bulldog Shale. Values obtained could then further analyse the potential on these faults as transport mechanisms allowing for secondary mineralisation within the proposed grabens.

Biogeochemical sampling along transects orientated west to east could also be used to further highlight potential drill site targets. Comparisons between the different geochemical assay results for the horsts and grabens, would particularly be useful in assessing the potential for secondary mineralisation within the proposed grabens. This method was found to be previously successful in identifying uranium mineralisation within Bulldog Shale grabens at Four Mile (Hill and Hore 2010).

Comparisons between opal presences and distribution at Coober Pedy could further support the opal exploration model proposed in this study. Coober Pedy is an opal mining town located north of Andamooka with similar Mesozoic sediments (i.e. Bulldog Shale) hosting opal mineralisation (Pewkliang *et al.* 2008). Evaluating the distribution of opal (based on opal diggings) and the digital elevation model for the region could further support the theory that opalisation is constricted to pyrite rich units which have been uplifted and consequently oxidised.

5. Conclusion

This study has shown the importance of understanding the landscape evolution for an area, in particular the acknowledgement of regolith and sedimentary cover material, previously considered an obstacle when exploring potentially mineral enriched basement geology. The cover material (Mesozoic sediments) in Andamooka is host to rich opalisation hereby predicted to have formed on exhumed fault blocks, caused by extensional intracontinental faults. The opal distribution previously was independently linked to fluctuating water tables, however oxidation of pyrite combined with varying water table height provides an enhanced interpretation linking opal distribution with jasper and silcrete lag material also present in the area.

ASTER band ratios and relative absorption-band depth ratios were found to assist in the production of a regolith-landform map with ratios primarily useful in distinguishing high reflectance homogenous mineral groups e.g. opal diggings, sand dunes. Differences between heterogeneous and homogenous mineral groups were also strongly distinguishable based on mean pixel colours. Additionally, landforms were easily identifiable based on similar linear pixels representing structures such as drainage depressions, longitudinal dunes and possibly faults.

The potential for further economic mineralisation (e.g. IOCG) is also proposed for Andamooka. With a source material (Olympic IOCG Province), transport mechanism (extensional duplex faulting), and potential trap rock (REDOX boundaries and varying permeability of Mesozoic units) all contributing to a prospective exploration model for the area.

6. Acknowledgements

A first thanks goes to my supervisor Robert Dart, for his wealth of knowledge, sense of humour and endless patience, which was severely tested throughout the year. To Steve Hill, thanks for your brief but very helpful time, and for the memorable field trip to the Yorke Peninsula (I will never look at sauce the same again). Thanks must also go to Georgina Gordon and Alan Mauger who helped significantly with the Hylogger data preparation and analysis found in this study. Thank you to Ken Clarke, for the encouragement I was heading in the right direction, when the fog started to come. To Oliver Hughes, thank you for your patience and driving expertise, particularly whilst I was incarcerated in a cast. I look forward to working with both you and Robert Klæbe in our future business adventures with Megalith and Varietea. Special thanks to Frank, for making me believe in myself as a geologist and potential botanist. Most importantly of all, thank you to Blair Pellegrino for the endless editing (sometimes brutal but necessary), meals, hugs and laughs. I really couldn't have done it without you and hope you know this thesis is as much yours as it is mine.

A geologist's life would be a happy one if he had only to drink, and never to write.

7. References

- BELPERIO A., FLINT R. & FREEMAN H. 2007. Prominent Hill: A hematite-dominated, iron oxide copper-gold system. *Economic Geology* **102**, 1499.
- BELPERIO A. P. & FLINT R. B. 1993. Geological note: The southeastern margin of the Gawler Craton. *Australian Journal of Earth Sciences* **40**, 423-426.
- BHATTACHARYA J. P. 1993. The expression and interpretation of marine flooding surfaces in core; examples from the Upper Cretaceous Durwegan Formation, Alberta Foreland Basin, Canada. *In*: Posamentier H. W., Summerhayes C. P., Haq B. U. & Allen G. P. eds., *Sequence Stratigraphy and Facies Associations*, Vol. 18, pp 125-160, International Association of Sedimentologists, Special Publication.
- CAMPBELL R. J. & HAIG D. W. 1999. Bathymetric change during Early Cretaceous intracratonic marine transgression across the northeastern Eromanga Basin, Australia. *Cretaceous Research* **20**, 403-446.
- CARR S. G., OLLIVER J. G., CONOR C. H. H. & SCOTT D. C. 1979. *Andamooka Opal Fields: The Geology of the Precious Stones Field and the Results of the Subsidised Mining Program*. Geological Survey of South Australia Department of Mines and Energy.
- CRAIG M. A., WILFORD J. R. & TAPLEY I. J. 1999. Regolith-landform mapping in the Gawler Craton. *Mesa Journal* **12**, 17-21.

- CROWLEY J. K., BRICKEY D. W. & ROWAN L. C. 1989. Airborne imaging spectrometer data of the Ruby Mountains, Montana: mineral discrimination using relative absorption band-depth images. *Remote Sensing of Environment* **29**, 121-134.
- DAY R. W. 1974. *Aptian ammonites from the Eromanga and Surat basins, Queensland* (Vol. 360). Dept. of Mines.
- DONOVAN A. D. 1993. The use of sequence stratigraphy to gain new insights into stratigraphic relationships in the Upper Cretaceous of the US Gulf Coast. *Sequence Stratigraphy and Facies Associations*, 563-577.
- EXON N. F. & SENIOR B. R. 1976. The Cretaceous of the Eromanga and Surat Basins. *BMR Journal of Australian Geology and Geophysics* **1**, 33-50.
- HARRIS W. K. 1962. Plant remains of Upper Jurassic to Lower Cretaceous age from Cadlareena military sheet. South Australia. *South Australia. Department of Mines. Report Book* **55**, 128.
- HART B. S. & PLINT A. G. 1993. Origin of an erosion surface in shoreface sandstones of the Kakwa Member (Upper Cretaceous Cardium Formation, Canada): importance for reconstruction of stratal geometry and depositional history. *Sequence Stratigraphy and Facies Associations*, 451-468.
- HEWSON R., KOCH C., BUCHANAN A. & SANDERS A. 2002. Detailed geological and regolith mapping in the Bangemall Basin, WA, using ASTER multi-spectral satellite-borne data.
- HILL S. M. & HORE S. B. 2010. Overview of Regolith and Landscape Evolution of the Arkaroola Wilderness Sanctuary, northern Flinders Ranges, South Australia.

- JABLONSKI D. 1987. Heritability at the species level: analysis of geographic ranges of Cretaceous mollusks. *Science* **238**, 360.
- JACKSON J. A. 1997. *Glossary of geology*. American Geological Institute, Alexandria, USA.
- JOHNS R. K. 1968. *Geology and mineral resources of the Andamooka-Torrens area*. Govt. Printer.
- KALINOWSKI A. & OLIVER S. 2004. ASTER Mineral Index Processing Manual. *Remote Sensing Applications, Geoscience Australia* **37**.
- LAMBERT I. B., KNUTSON J., DONNELLY T. H. & ETMINAN H. 1987. Stuart Shelf-Adelaide Geosyncline copper province, South Australia. *Economic Geology* **82**, 108-123.
- LEITHOLD E. L. 1994. Stratigraphical architecture at the muddy margin of the Cretaceous Western Interior Seaway, southern Utah. *Sedimentology* **41**, 521-542.
- LUDBROOK N. H. 1966. *Cretaceous biostratigraphy of the Great Artesian Basin in South Australia*. WL Hawes, Govt. Printer.
- LUDBROOK N. H. 1967. Stuart Range No. 3 Bore—Coober Pedy. Stratigraphy and micropalaeontology. *Mining Review, Adelaide* **122**, 28-31.
- MAH A. 2002. *ASTER wizard of ER Mapper*. Waclawik V. G., Perth, Western Australia.
- MAHONEY S., JAMES P., MAUGER A. & HEINSON G. 2002. Geologic and regolith mapping for mineral exploration in the Gawler Craton of South Australia using hyperion and other remote sensing techniques, pp. 1779-1781. IEEE.

- MAUGER A. J., KEELING J. L. & HUNTINGTON J. F. 2004. Bringing remote sensing down to earth: CSIRO HyLogger as applied in the Tarcoola Goldfield, South Australia.
- MORRIS B. J. & ZHE J. 2010. High resolution resistivity test survey: Andamooka. *PIRSA Geological Survey Branch*.
- NINOMIYA Y. & FU B. 2001. Spectral indices for lithologic mapping with ASTER thermal infrared data applying to a part of Beishan Mountains, Gansu, China, pp. 2988-2990 vol. 2987. IEEE.
- NUMMEDAL D. & MOLENAAR C. M. 1995. Sequence stratigraphy of ramp-setting strand plain successions: the Gallup Sandstone, New Mexico. *MEMOIRS-AMERICAN ASSOCIATION OF PETROLEUM GEOLOGISTS*, 277-310.
- PAIN C. F. 2008. Field Guide for Describing Regolith and Landforms CRC LEME. *CSIRO Exploration and Mining, PO Box 1130*, 94.
- PEWKLIANG B., PRING A. & BRUGGER J. 2008. The formation of precious opal: clues from the opalization of bone. *The Canadian Mineralogist* **46**, 139-149.
- POWELL C. M. A., ROOTS S. R. & VEEVERS J. J. 1988. Pre-breakup continental extension in East Gondwanaland and the early opening of the eastern Indian Ocean. *Tectonophysics* **155**, 261-283.
- RABUS B., EINEDER M., ROTH A. & BAMLER R. 2003. The shuttle radar topography mission--a new class of digital elevation models acquired by spaceborne radar. *ISPRS Journal of Photogrammetry and Remote Sensing* **57**, 241-262.

- REYNOLDS S. D., COBLENTZ D. D. & HILLIS R. R. 2003. Influences of plate-boundary forces on the regional intraplate stress field of continental Australia. *SPECIAL PAPERS-GEOLOGICAL SOCIETY OF AMERICA*, 59-70.
- ROGERS P. A. & FREEMAN P. J. 1993. *Explanatory notes for the Warrina 1:250 000 geological map*. Department of Mines and Energy/Geological Survey South Australia, Adelaide.
- ROWAN L. C. & MARS J. C. 2001. Initial lithologic mapping results using advanced spaceborne thermal emission and reflection radiometer (ASTER) data.
- ROWAN L. C. & MARS J. C. 2003. Lithologic mapping in the Mountain Pass, California area using advanced spaceborne thermal emission and reflection radiometer (ASTER) data. *Remote Sensing of Environment* **84**, 350-366.
- SANDIFORD M. 2003. Neotectonics of southeastern Australia: linking the Quaternary faulting record with seismicity and in situ stress. *SPECIAL PAPERS-GEOLOGICAL SOCIETY OF AMERICA*, 107-120.
- SENIOR B. R., MOND A. & HARRISON P. L. 1978. *Geology of the Eromanga Basin*. Australian Govt. Pub. Service.
- SKIRROW R. G. & DAVIDSON G. J. 2007. A Special Issue Devoted to Proterozoic Iron Oxide Cu-Au-(U) and Gold Mineral Systems of the Gawler Craton: Preface. *Economic Geology* **102**, 1373-1375.
- SPRIGG R. C. & LTD S. O. T. G. A. 1958. The Great Artesian Basin in South Australia. *The Geology of South Australia. Geological Society of Australia* **5**, 88-101.
- TAYLOR G. & EGGLETON R. A. 2001. *Regolith geology and geomorphology*. Wiley.

- TWIDALE C. R. 1972. Landform development in the Lake Eyre region, Australia. *Geographical Review*, 40-70.
- TWIDALE C. R. & CAMPBELL E. M. 1991. The early Cretaceous marine transgression and its significance for landscape interpretation. *The Australian Geographer* **22**, 178-184.
- VEEVERS J. J. 2006. Updated Gondwana (Permian-Cretaceous) earth history of Australia. *Gondwana Research* **9**, 231-260.
- WACLAWIK V. G. 2006. Landscape evolution of the Umbum Creek Catchment, Western Lake Eyre, Central Australia.
- WETHERBY K. 2006. *Revised soil description book*. Masters Agricultural Science, Adelaide.
- WOPFNER H. 1964. Permian-Jurassic history of the western Great Artesian basin. *Transactions of the Royal Society of South Australia* **88**, 117-128.
- WOPFNER H. 2010. burial history of Jurassic gondwana surface west and southwest of lake Eyre, central Australia. *Cadernos do Laboratorio Xeolóxico de Laxe*, 221-242.
- WOPFNER H., FREYTAG I. & HEATH G. 1970. Basal Jurassic-Cretaceous rocks of western Great Artesian Basin, South Australia: stratigraphy and environment. *American Association of Petroleum Geologists Bulletin* **54**, 383-416.
- WOPFNER H. & TWIDALE C. R. 1967. Geomorphological history of the Lake Eyre basin. *Landform Studies from Australia and New Guinea*, 118-143.

8. Figure captions

Figure 1: Locality map of Andamooka in regards to Australia, South Australia, and the discovered IOCG deposits

Figure 2: Interpreted geological map of Andamooka edited from Geological Survey of South Australia grid map SH 53-12 (05 Oct 1999)

Figure 3: Section through the Algebuckina Sandstone (Wopfner *et al.* 1970)

Figure 4: Section through the Cadna-owie Formation (Wopfner *et al.* 1970)

Figure 5: Cross section through Bulldog Shale showing common location of opalisation (Carr *et al.* 1979)

Figure 6: Electromagnetic reflectance values recorded by the ASTER sensor onboard the Terra Satellite (Kalinowski and Oliver 2004)

Figure 7: Explanation of the regolith-landform codes, using channel sediments deposited on a river flood plain as an example (Craig *et al.* 1999)

Figure 8: Location of soil and lag grab samples taken in Andamooka during first field trip (11 April 2011 to 13 April 2011)

Figure 9: Guidelines to classifying soil textures by Wetherby (2006)

Figure 10: Example of spectral signatures for kaolinite, illite-smectite, gypsum, and alunite recorded over the Tarcoola area (Mahoney *et al.* 2002)

Figure 11: Andamooka regolith-landform map for study area (for a detailed description of the individual RLUs, view Table 2)

Figure 12: *In-situ* exposures of horizontally bedded massive crystalline quartzite i.e. Arcoona Quartzite (observed at 715769 E and 6627544 N)

Figure 13: Exposed Arcoona Quartzite observed at steeply dipping angle approximately 500m west of previous photo. Angular beds strongly orientated in northeast to southwest orientation. Also noted with a reduction in quartz grain sizes (observed at 715116 E and 6627897 N)

Figure 14: Handheld close up of gypsum (a) and kaolinite (c) rich soil immediately adjacent to angular bedded quartzite. Photo of these soils in situ (b & d) (715144 E 6627896 N)

Figure 15: Regolith-landform map for Andamooka showing predicted extensional faults orientation NE-SW along present drainage depressions

Figure 16: Cross section from A to B showing predicted lithologies and structures

Figure 17: Iron rich veins within the Bulldog Shale percolating down unit

9. Figures

Figure 1

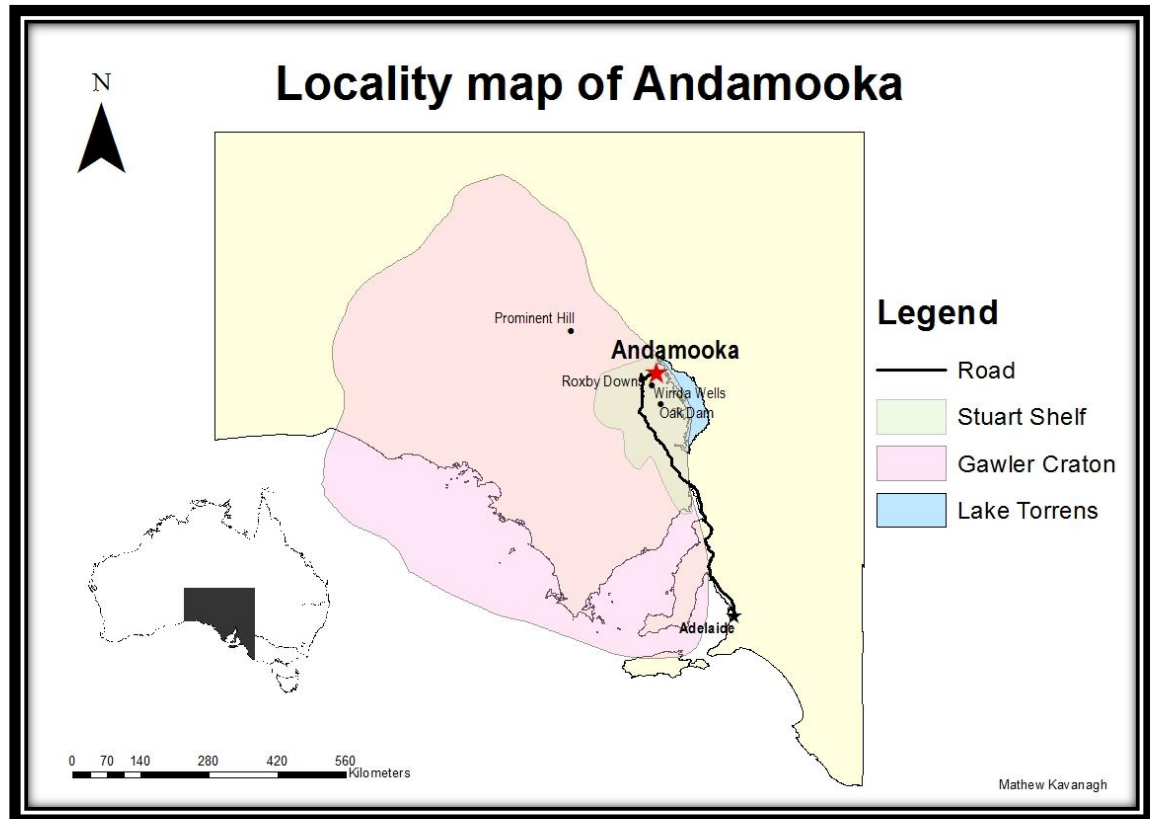
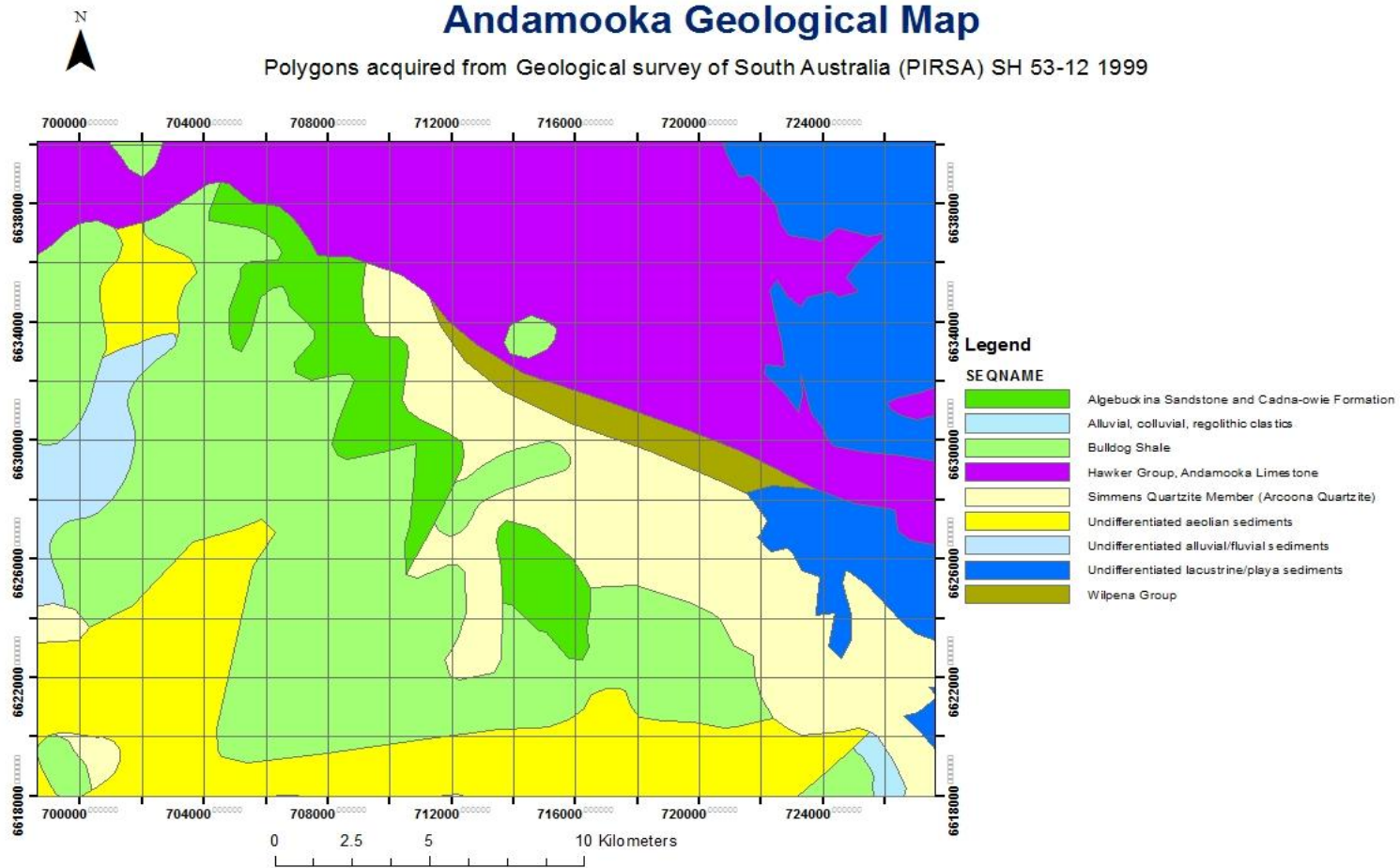


Figure 2



Author: Mathew Kavanagh

Coordinate System: GDA 1994 MGA Zone 53 Transverse Mercator

Date: 21/09/2011

Figure 3

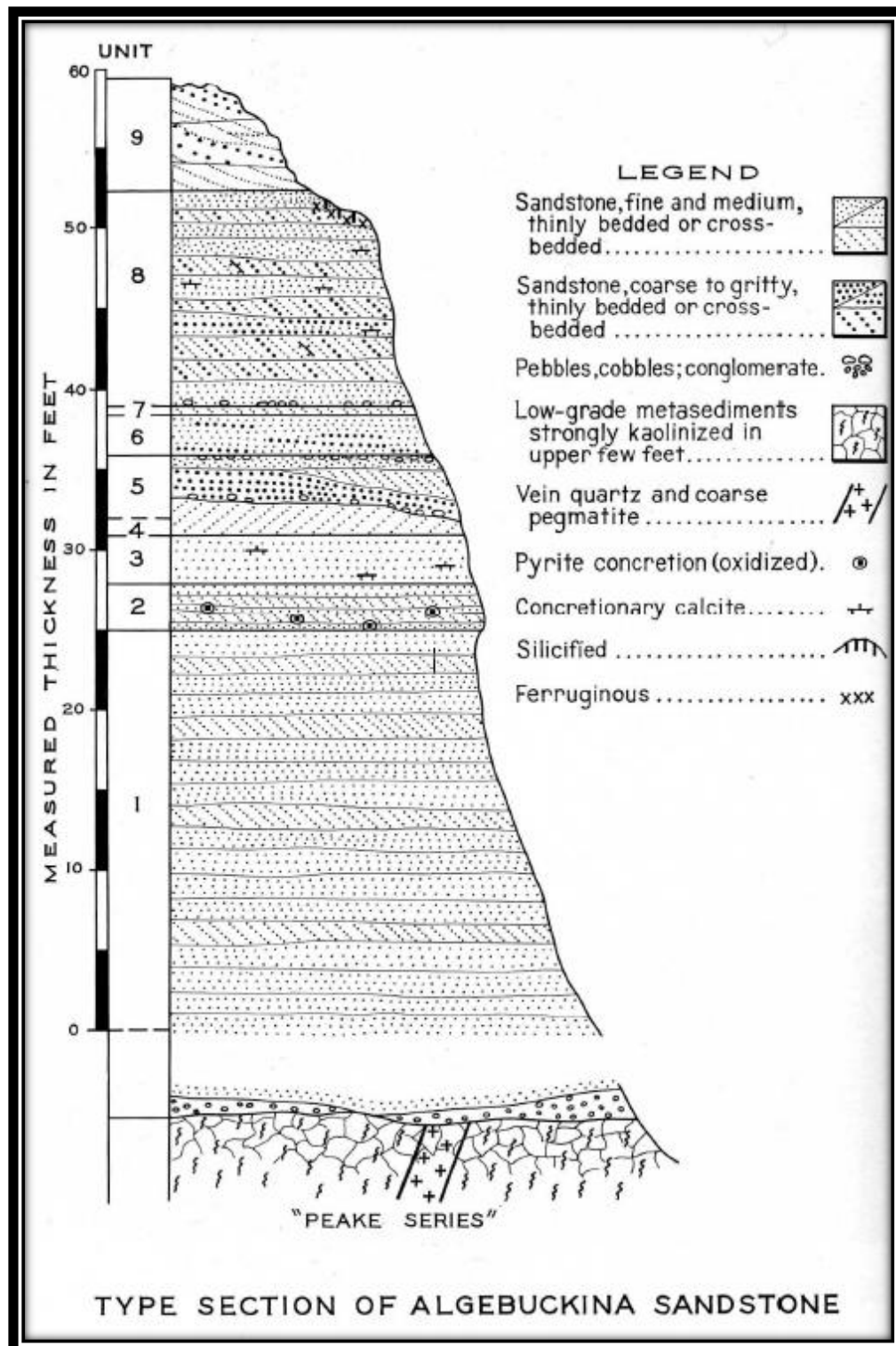


Figure 4

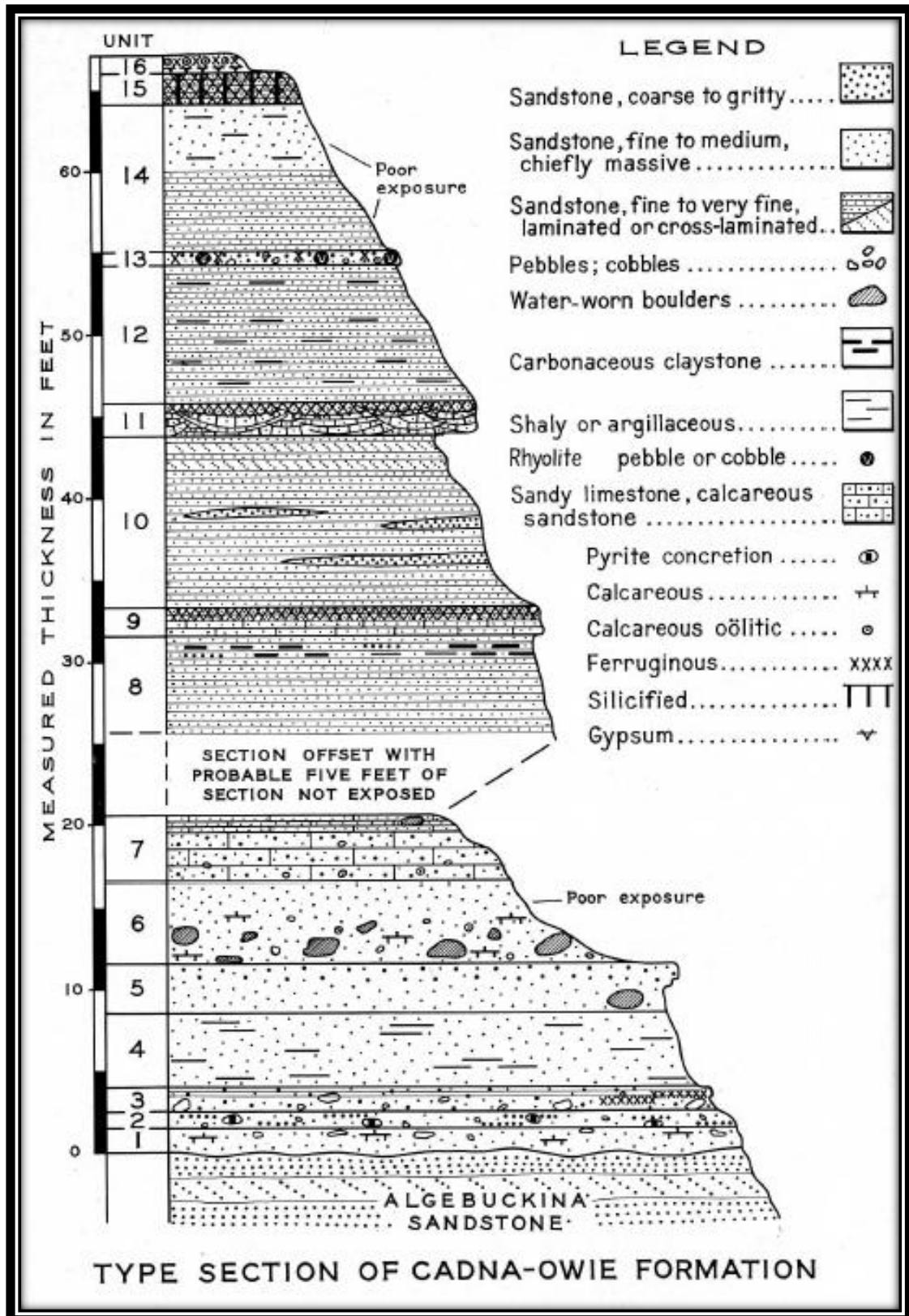


Figure 5

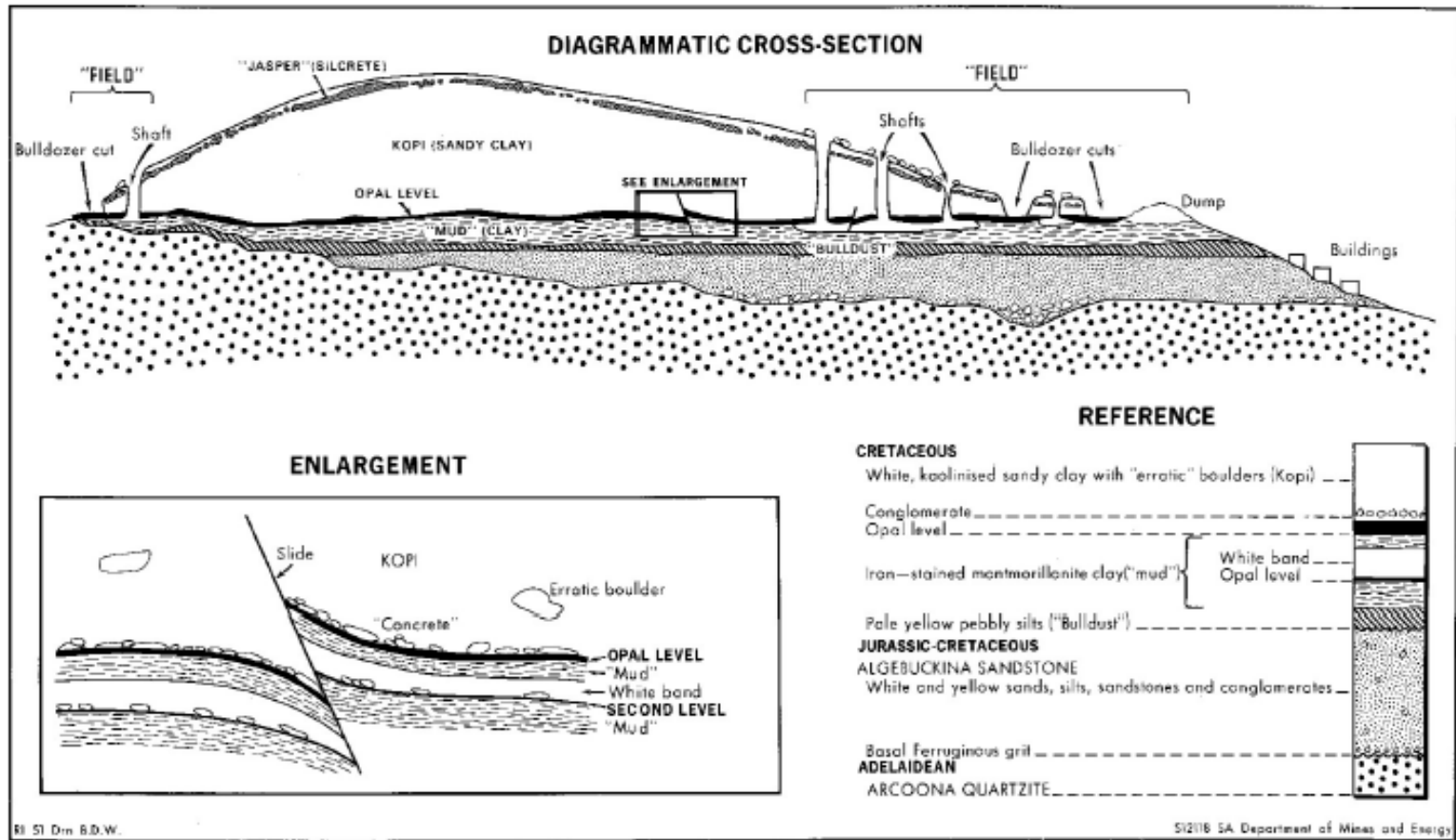


Figure 6

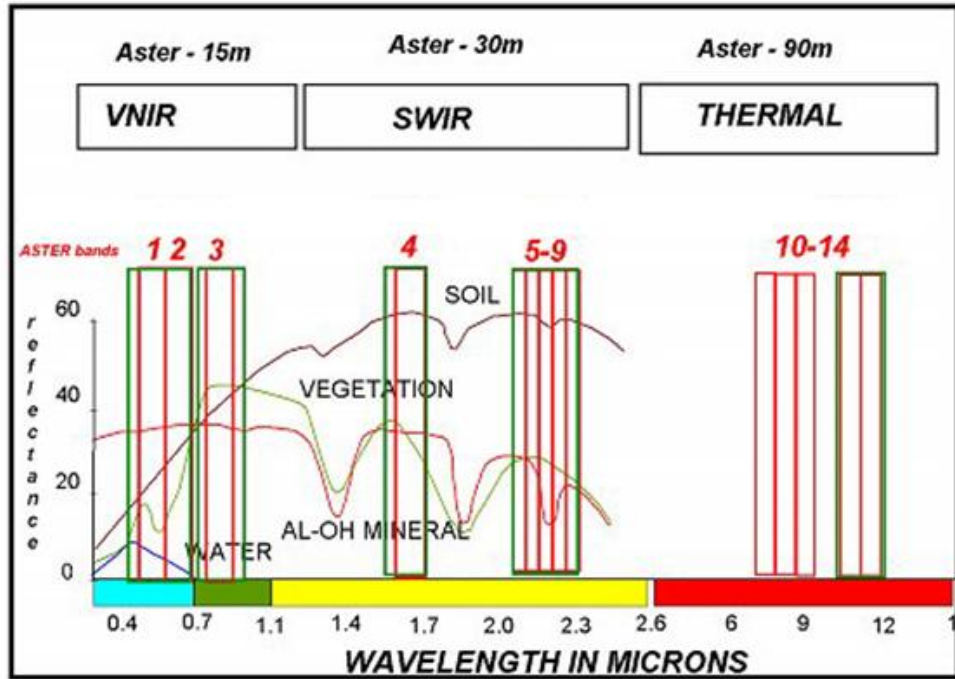


Figure 7

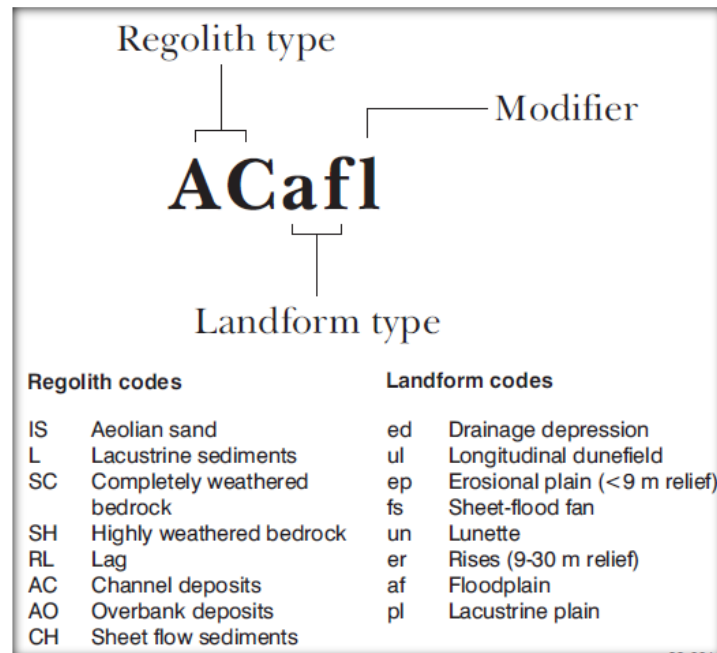


Figure 8

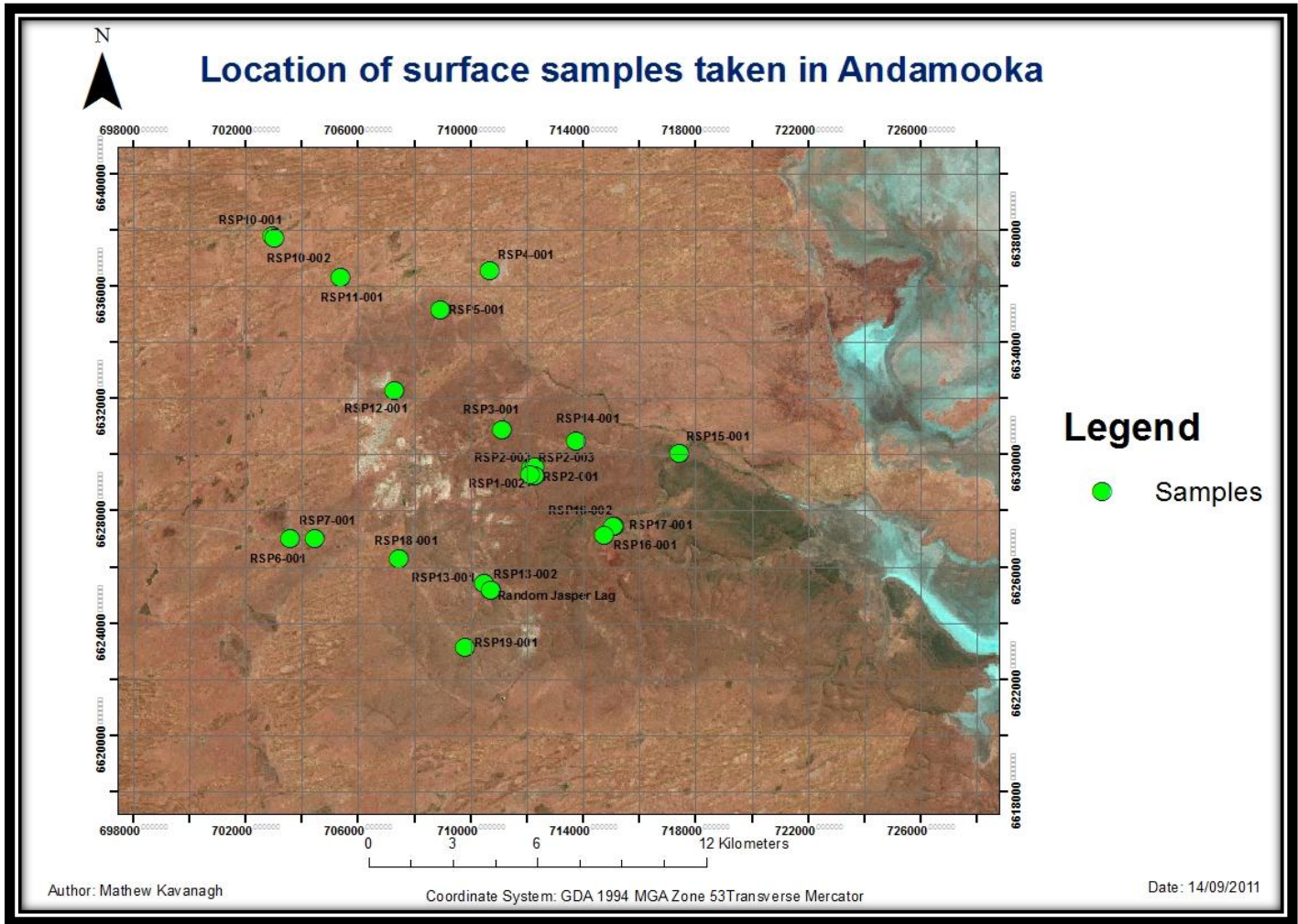


Figure 9

Symbol	Description
(S)	<u>SAND</u> Coherence nil to very slight, cannot be moulded: single grains adhere to fingers: nil to very slight turbidity when puddled.
(LS)	<u>LOAMY SAND</u> - will form ribbon to 5mm. Slight coherence; definite turbidity when puddled in hand.
(CS)	<u>CLAYEY SAND</u> - Will form ribbon 5 to 15 mm. Slight coherence; sticky when wet, many sand grains stick to fingers; discolours fingers with clay stain.
(SL)	<u>SANDY LOAM</u> - Will form ribbon of 15 to 20 mm. Bolus coherent and very sandy to touch; sand grains visible.
(LSCL)	<u>LIGHT SANDY CLAY LOAM</u> - Will form ribbon of 20 to 25 mm. Bolus moderately coherent but sandy to touch; sand grains easily visible.
(L)	<u>LOAM</u> Bolus coherent and spongy; smooth feel and no obvious sandiness; may feel somewhat greasy as organic matter is usually present. Will form ribbon of about 25mm.
(SCL)	<u>SANDY CLAY LOAM</u> - Will form ribbon 25 to 40 mm. Bolus strongly coherent, sandy to touch; sand grains visible.
(CL)	<u>CLAY LOAM</u> - Will form ribbon 40 to 50 mm. Bolus strongly coherent and plastic; smooth to manipulate.
(SC & LC)	<u>SANDY CLAY and LIGHT CLAY</u> - Will form ribbon 50 to 75 mm. Plastic bolus, slight resistance to shearing. SC - can see, feel and hear sand grains. LC - smooth to touch.
(LMC)	<u>LIGHT MEDIUM CLAY</u> - Will form ribbon 75 to 85mm. Plastic bolus; smooth to touch; moderate resistance to shearing between thumb and forefinger.
(MC)	<u>MEDIUM CLAY</u> - Will form ribbon 85 to 100mm. Smooth plastic bolus; handles like plasticine and can be moulded into rods; moderate resistance to ribboning.
(HC)	<u>HEAVY CLAY</u> - Will easily form ribbon over 100mm. Smooth plastic bolus; handles like stiff plasticine; can be moulded into rods without fracture; has firm resistance to ribboning shear.

Figure 10

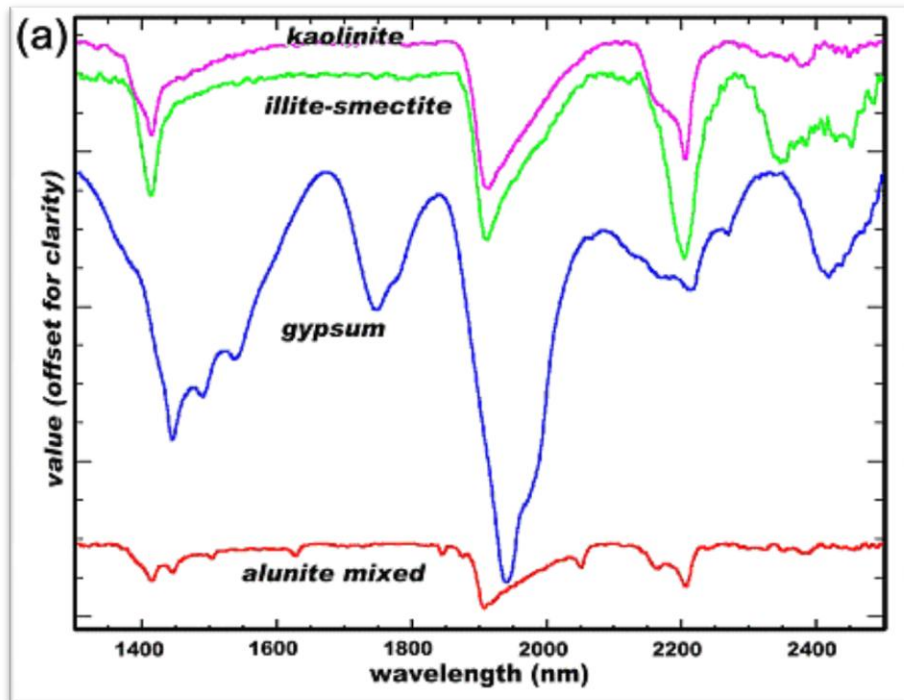


Figure 11 (see Table 2 for description of RLUs)

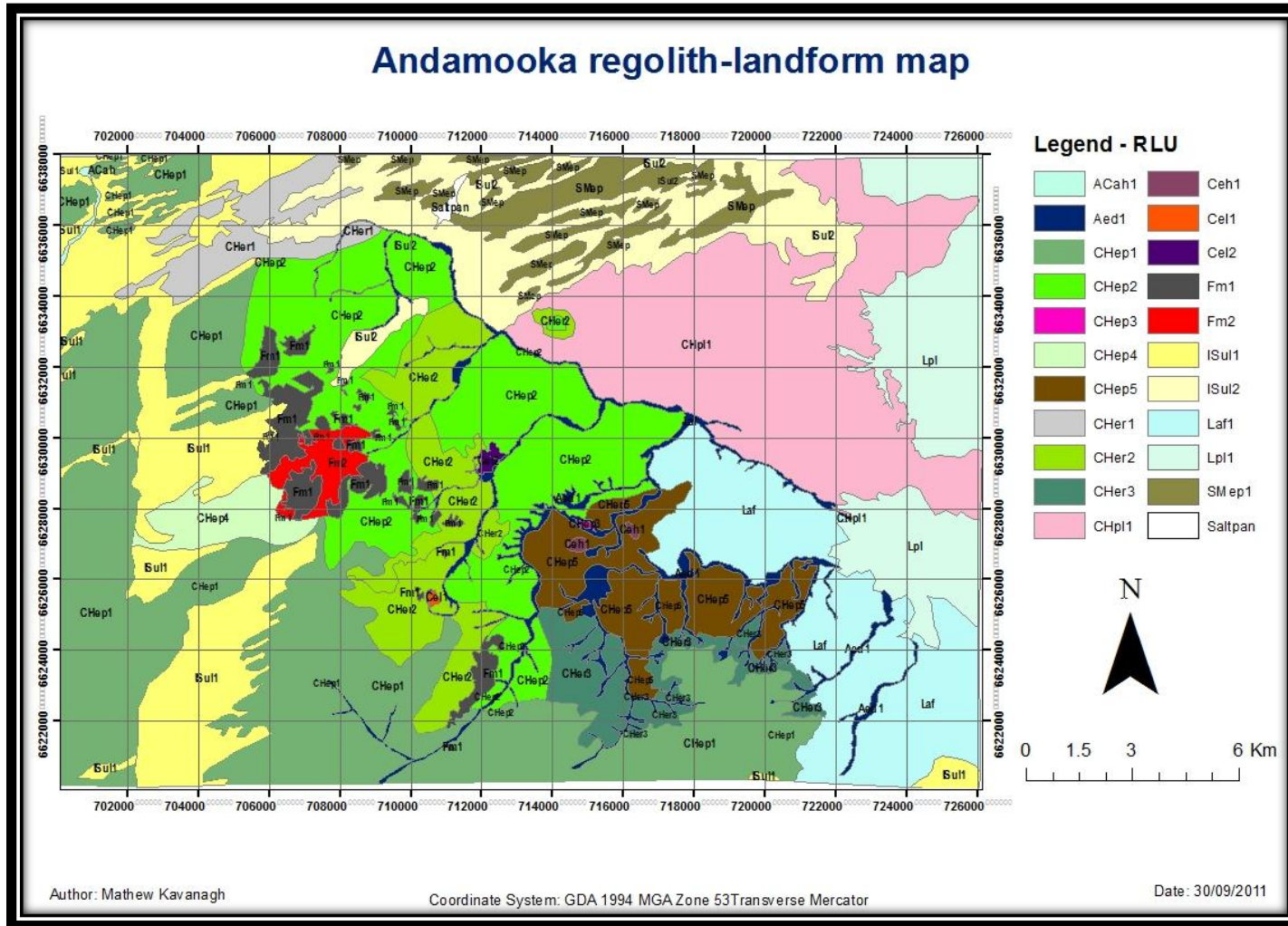


Figure 12



Figure 13



Figure 14

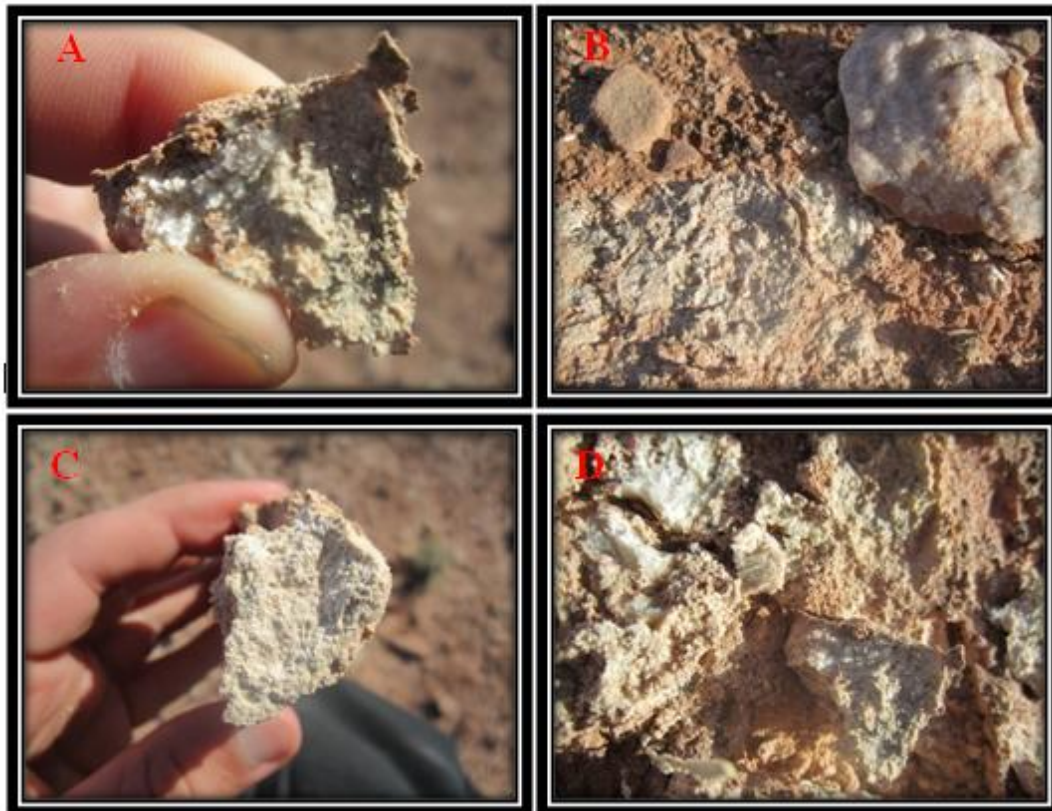


Figure 15

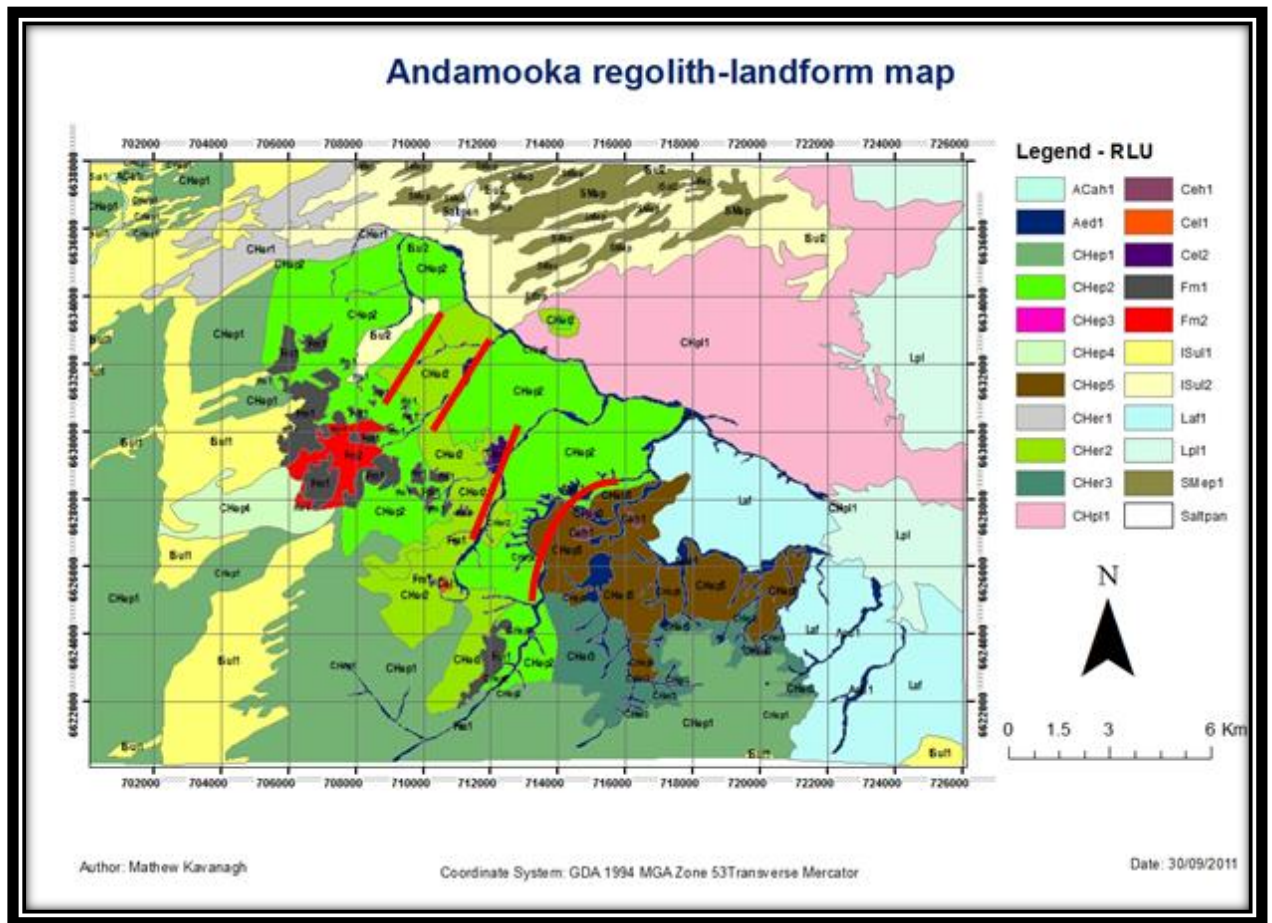


Figure 16

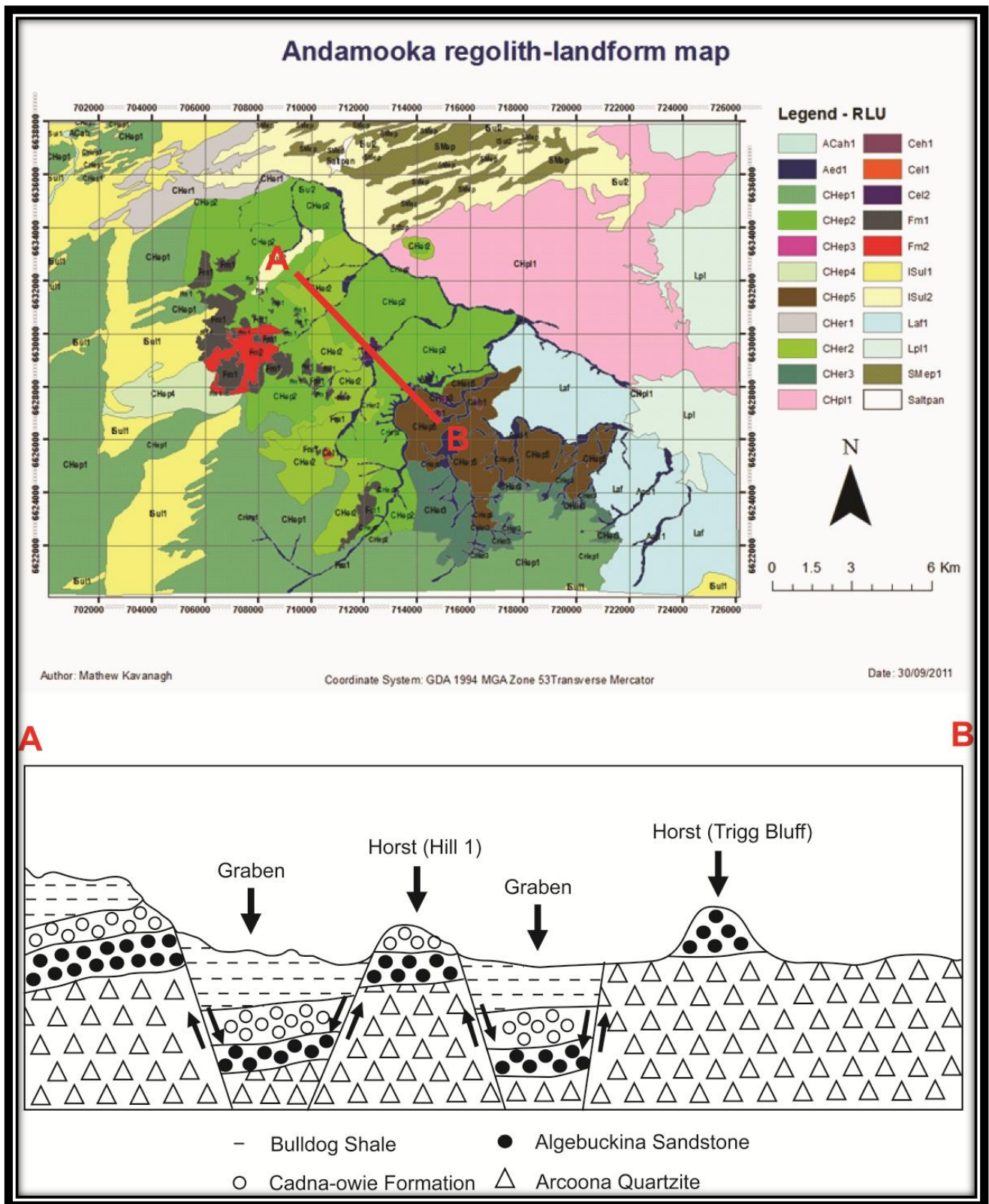


Figure 17






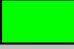



10. Tables





Table 1 Common ratio and band combinations




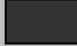

Features	Red	Green	Blue	Reference
True colour	3	2	1	
Iron oxides, ferrous iron, clays	3/2	3/7	4/7	CSIRO Regolith Ratios
Clays, amphibole, laterite	$(5 \times 7)/6^2$	6/8	4/5	Bierwith
Silica, carbonate, basic degree index	$(11 \times 11)/10/12$	13/14	12/13	Bierwith
Enhanced structural features	7	4	2	Rowan (USGS)
Carbonate, clays, siliceous rocks	13/14	$(5 \times 7)/6^2$	$(11 \times 11)/(10 \times 12)$	Bierwith, Nimoyima, CSIRO
Al-OH minerals/advanced argillic alteration, alunite/pyrophyllite, mica, kaolinite/dickite	5/6 (phen)	7/6 (musc)	7/5 (kaol)	Hewson CSIRO
Discrimination for mapping	4/1	3/1	12/14	Abdelsalam


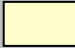
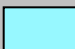
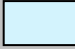

Table 2 Detailed RLU legend

Landform	Classification
ACah₁ 	Alluvial channel depositing fine grained sediments in a low energy river system when filled with water. Abundance of vegetation with high canopy cover.
Aed₁ 	Alluvial drainage depressions with general flow direction from north west to south east. Abundance of reworked rounded sediments from the upper plains, including quartzite pebbles, pink shales and conglomerates. Note the abundance of kaolinite and lack of sand within the poorly structured soils along drainage beds. Easily identifiable by the abundance of vegetation in a linear orientation. Vegetation includes high density Bullock Bush (<i>Alectryon aleifolius</i>), Western Myall (<i>Acacia papyrocarpa</i>), bluebush (<i>Maireana</i> spp.), grasses, <i>Malva</i> sp., and saltbush (<i>Atriplex</i> and <i>Rhagodia</i> spp.).
CHep₁ 	Sheet flow erosional plain adjacent to sand dunes. As plains are on the crest of the sand dunes, abundance of sand is noted in the soil matrix with a kaolinite clay and hematite component noted within the ribboning and Hylogger data. Lag includes varying grain shape and sizes of silcrete (jasper), quartzite, small hematite angular nodules, rounded quartz fragments, silicified conglomerates with small rounded quartz clasts and potch opal closer to opal diggings. Vegetation includes acacias and bluebushes.

<p>CHep₂</p> 	<p>Sheet flow erosional plain further away from sand dunes. Soil contains abundance of clay and loam with a greater soil structure noted than adjacent plains. Lag includes sub-angular to rounded iron stained quartzite (1-20 cm), rounded silcrete (2-10 cm), thinly layered flat quartzite (5-10 cm), rounded fluvial pebbles, potch opal, cemented kaolinite pebbles small rounded hematite and goethite nodules. Importantly the opal diggings are found predominantly within this RLU with the majority found within the higher elevated CHep₂ units. Vegetation includes saltbush (<i>Atriplex and Rhagodia</i> spp.), long-spined bindyi (<i>Sclerolaena longicuspis</i>) and grasses. This unit comprises up part of the Bulldog Shale.</p>
<p>CHep₃</p> 	<p>Sheet flow erosional plain surrounded by drainage depressions and consequently influenced by flooding. Soil contains abundance of clay minerals montmorillonite and kaolinite leading to a low porosity, good structured soil. Surface contains an abundance of mud cracks caused by clays shrinking and swelling. Red soil granules also observed on the surface. Lag includes, silcrete, goethite, gypsum, blocky quartzite with muscovite grains, and small rounded pebbles. Vegetation includes chenopods (<i>Rhagodia, Atriplex and Maireana</i> spp.).</p>
<p>CHep₄</p> 	<p>Sheet flow erosional plain, adjacent to road. Despite the plains proximity to sand dunes the soil contains an abundance of clay and loam evident by ribbon of soil and shrink swell cracks on surface. Loam material probably sourced from abundance of vegetation on adjacent sand dunes. Lag includes small iron rich (goethite) quartzite pebbles (only on surface), siderite, and silcrete.</p>
<p>CHep₅</p> 	<p>Sheet flow erosional plain closest towards Lake Torrens. Light coloured red - brown sandy soil with relatively high porosity. Lag includes characteristically abundant flat angular quartzite lag (presumably sourced from Arcoona quartzite lithology). Patches of outcropping Arcoona found within plain (too small for an individual unit), bedded at a unique angular angle immediately adjacent to horizontal outcropping beds. Angular bedded units orientated in a NE-SW linear direction, indicating possible faulting in the area. Light patches of soil observed around these faults, with an abundance of gypsum. Vegetation include saltbush (<i>Atriplex and Rhagodia</i> spp.), bluebush (<i>Maireana</i> spp.), senna (<i>Senna artemisioides</i>) and <i>Malva</i> sp.</p>

CHer₁ 	<p>Sheet flow erosional rise gradually sloping downwards in a south easterly direction. Sandy clay soil texture with montmorillonite and kaolinite grains producing a granular structure soil. Lag consists of angular Fe-rich silcrete (5-15 cm), grains of muscovite and magnesite minerals present.</p>
CHer₂ 	<p>Sheet flow erosional rise between higher elevated CHep₂ (to the west) and lower elevated CHep₂ (to the east). Lower slopes of rise contain patches of outcropping Cadna-owie beach sands with patches of ferruginous members. Upper part of the rises contain carbonates with fine clay and mud sediments indicative of Bulldog Shale formation. Variety of lag observed including, rounded quartz pebbles, angular silcrete and silicified breccias. Upper slope of rises characteristically distinguishable by light white coloured soil. Vegetation includes bluebush (<i>Maireana</i> spp.), senna (<i>Senna artemisioides</i>), <i>Malva</i> sp., long-spined bindyi (<i>Sclerolaena longicuspis</i>) and grasses.</p>
CHer₃ 	<p>Sheet flow erosional rise concentrated to the south east of mapping area. Sheet flow movement controlled by water drainage along steep slopes, percolating towards Lake Torrens. Lag consists of a combination of lag from higher plains with an abundance of Arcoona sub-rounded quartzite.</p>
CHpl₁ 	<p>Sheet flow on a lacustrine plain as higher elevated material from the west is deposited on flat plain adjacent to Lake Torrens. Abundance of salt associated with plain and variety of lag (similar to CHer₃) observed.</p>

<p>Ceh₁</p> 	<p>Colluvial hill named Trig Bluff. Outcropping Algebuckina Sandstone observed along slopes with the lower unit consisting of moderately well sorted fine to medium grained kaolinitic sandstone, with angular to sub angular milky to clear quartz grains. Pyrite concretions and pebble conglomerate units appear mid way through the unit with angular current bedding. The upper part of the unit is characterized by ferruginous layers leading to very well sorted clean semifriable quartz sandstone (quartz arenite), with silicification producing a quartzitic crust. Fossilized ferns are noted within the clean quartz arenite top unit. Lag at the top of Bluff includes rounded fluvial pebbles, sub-rounded quartzite, silcrete, angular sandstone and ferruginous nodules. Vegetation includes bluebush (<i>Maireana</i> spp.), senna (<i>Senna artemisioides</i>), saltbush (<i>Atriplex</i> and <i>Rhagodia</i> spp.) and grasses.</p>
<p>Cel₁</p> 	<p>Colluvial low hill. Abundance of kaolinite cover (possibly Kopi from opal diggings) and gypsum lag, indicative of Bulldog Shale formation. Notably adjacent to opal diggings.</p>
<p>Cel₂</p> 	<p>Colluvial low hill adjacent to Blue Dam. Multiple outcrops of the Cadna-owie Formation observed within drainage depressions down slope of hill (eastern side). Outcrops include well sorted sandstones and kaolinite at the bottom, ferricrete, carbonaceous and pyrite concretions appearing in the middle units, and silicified conglomerates capping the top. Lag includes silicified conglomerates with rounded quartz clasts, rounded blocky crystalline quartzite, silcrete and ferruginous nodules. Vegetation on top of hill includes bluebush (<i>Maireana</i> spp.), <i>Malva</i> sp., senna (<i>Senna artemisioides</i>), long-spined bindyi (<i>Sclerolaena longicuspis</i>) and grasses.</p>
<p>Fm₁</p> 	<p>Man made, opal diggings.</p>
<p>Fm₂</p> 	<p>Man made, Andamooka town centre.</p>

ISul₁ 	Longitudinal sand dunes located in the west of mapping area adjacent to CHep ₁ . Unit consists of aeolian deposited quartz sands with an abundance of iron present within the unit. RLU distinguishable by abundance of diverse vegetation which includes bluebushes, Cyprus pines and Acacias.
ISul₂ 	Longitudinal sand dunes located in north of mapping area with a carbonate influence (observed by patches of white calcrete within the soil) due to presence of underlying limestone.
Laf₁ 	Lacustrine flood plain with overlying lag from the higher plains to the west.
Lpl₁ 	Dry endorheic rift saline basin termed Lake Torrens, depositing lacustrine fine salts and sediments.
SMep₁ 	Moderately weathered outcropping Andamooka Limestone, distinguishable by 'elephant skin' appearance and abundance of lichen overgrowth.

11. Appendices

Appendix 1

Surface soil and lag samples

Sample	Soil	Lag	Location	Landform	Texture	Colour	pH	Lag	Vegetation	Extra Notes
RSP1-001	Y	Y	0712171 E 6629524 N	Cel ₂	CL	2.5 Yr 4/8	5.5	Poorly sorted, ranging from well sorted alluvial pebbles (10-15 cm) to older sub-angular silcrete and angular quartzite cobbly in size (6-20 cm).	Grasses, saltbush, bluebush, long-spined bindyi	Iron rich red-brown soil. Sample taken on top of Hill 1, adjacent to Blue Dam
RSP1-002	Y	Y	0712278 E 6629535 N	Cel ₂	CS	2.5 Yr 4/8	5.5	Silicified conglomerates with rounded quartz clasts, rounded blocky crystalline quartzite, silcrete and ferruginous nodules.	Grasses, saltbush, bluebush	Bottom of Hill 1
RSP2-001	Y	Y	0712293 E 6629225 N	Cel ₂	LS	5 Yr 4/6	6.5	Silicified conglomerates with rounded quartz clasts, rounded blocky crystalline quartzite, silcrete and ferruginous nodules.	Shrubs, grasses, <i>Malva</i> sp.	Bottom of Hill 1 adjacent to ferruginous outcrop
RSP2-002	Y	Y	0712280 E 6629224 N	Cel ₂	LS	5 Yr 4/6	6	Silicified conglomerates with rounded quartz clasts, rounded blocky crystalline quartzite, silcrete and ferruginous nodules.	Shrubs, grasses	

Sample	Soil	Lag	Location	Landform	Texture	Colour	pH	Lag	Vegetation	Extra Notes
RSP2-003	Y	Y	0712132 E 6629294 N	Cel ₂	SL	7.5 Yr 4/4	5.5	Silicified conglomerates with rounded quartz clasts, rounded blocky crystalline quartzite, silcrete and ferruginous nodules.	Small shrubs, grasses, saltbush, bluebush	Fine brown soil taken on top of Hill 1 further south
RSP3-001	Y	Y	0711132 E 6630866 N	CHep ₂	CL	5 Yr 5/4	6.5	Sub-angular to rounded iron stained quartzite (1-20 cm), rounded silcrete (2-10 cm), thinly layered flat quartzite (5-10 cm), rounded fluvial pebbles, potch opal, cemented kaolinite pebbles small rounded hematite and goethite nodules.	Bladder / old man saltbush, copper-burrs	Fine brown soil occurrence of mud cracks, large plain area
RSP4-001	Y	Y	0710709 E 6636522 N	ISul ₂	S	5 Yr 5/4	8.5	Little limestone lag.	Acacia (Mulga), grasses, saltbush, bluebush	Sand dunes adjacent to outcropping Andamooka Limestone and Saltpan
RSP5-001	Y	Y	0708926 E 6635140 N	CHep ₂	LCL	5 Yr 5/4	6.5	Sub-angular to rounded iron stained quartzite (1-20 cm), rounded silcrete (2-10 cm), thinly layered flat quartzite (5-10 cm), rounded fluvial pebbles, potch opal, cemented kaolinite pebbles small rounded hematite and goethite nodules.	Chenopods	
RSP6-001	Y	Y	0703603 E 6626983 N	CHep ₄	SCL	5 Yr 5/4	9	Small iron rich (goethite) quartzite pebbles (only on surface), siderite, and silcrete.		

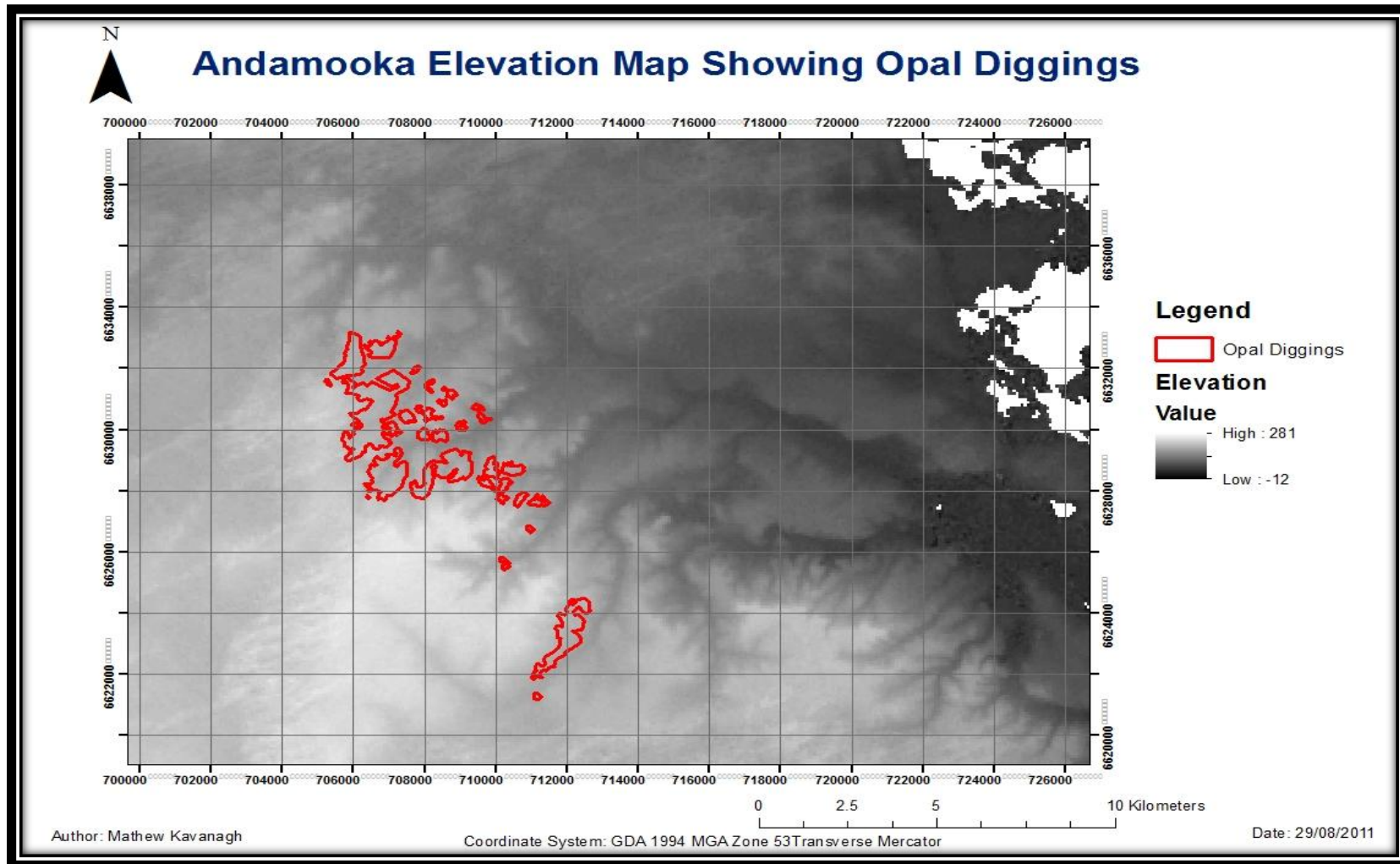
Sample	Soil	Lag	Location	Landform	Texture	Colour	pH	Lag	Vegetation	Extra Notes
RSP7-001	Y	N	0704468 E 6626991 N	ISul ₁	S	2.5 Yr 4/6	6	No lag.	Lots of vegetation variety, including <i>Acacia</i>	
RSP8-001	Y	Y	0693594 E 6626791 N	CHep	SCL	5 Yr 4/6	9-9.5	Flat angular crystalline quartzite (5-10 cm) with thin (2 mm) bedding preserved.	Grasses, bluebush	
RSP9-001	Y	N	0681178 E 6600519 N	ISul	S	10 R 4/8	7.5	No lag.		
RSP10-001	Y	N	0702946 E 6637772 N	ISul ₁	S	10 R 4/8	6	No lag.	<i>Acacia</i>	Crest of ISul1 unit on edge of plains (CHep ₁)
RSP10-002	Y	Y	0703041 E 6637684 N	CHep ₁	CS	2.5 Yr 4/6	7.5	Varying grain shape and sizes of silcrete (jasper), quartzite, small hematite angular nodules, rounded quartz fragments, silicified conglomerates with small rounded quartz clasts.	Bluebush	Boundary of CHep ₁ , adjacent to ISul units
RSP11-001	Y	Y	0705405 E 6636283 N	CHer ₁	SC	5 Yr 4/6	7	Angular Fe-rich silcrete (5-15 cm), grains of muscovite and magnesite minerals present.		Gradual rise from lower elevated CHep ₂ to higher elevated CHep ₂
RSP12-001	Y	Y	0707323 E 6632268 N	CHep ₂	CL	5 Yr 4/6	9	Sub-angular to rounded iron stained quartzite (1-20 cm), rounded silcrete (2-10 cm), thinly layered flat quartzite (5-10 cm), rounded fluvial pebbles, potch opal, cemented kaolinite pebbles small rounded hematite and goethite nodules.	Healthy flowering <i>Acacia</i>	Mud cracks observed on surface due to shrink swell of clay content

Sample	Soil	Lag	Location	Landform	Texture	Colour	pH	Lag	Vegetation	Extra Notes
RSP13-001	Y	Y	0710747 E 6625180 N	CHer ₂	SCL	5 Yr 4/6	7.5	Variety of lag observed including, rounded quartz pebbles, angular silcrete and silicified breccias.	Bluebush, senna, <i>Malva</i> sp., long-spined bindyi	
RSP13-002	Y	Y	0710481 E 6625407 N	Aed ₁	LC	7.5 Yr 6/3	6.5	Reworked rounded sediments from the upper plains, including quartzite pebbles, pink shales and conglomerates.		Poor soil structure, subject to slacking
RSP14-001	Y	Y	0713751 E 6630479 N	CHep ₂	LS	5 Yr 4/4	5.5	Sub-angular to rounded iron stained quartzite (1-20 cm), rounded silcrete (2-10 cm), thinly layered flat quartzite (5-10 cm), rounded fluvial pebbles, potch opal, cemented kaolinite pebbles small rounded hematite and goethite nodules.	Bluebush	Abundance of iron
RSP15-001	N	Y	0717428 E 6630042	Aed ₁ (SSep)	-	-	-	Flat Arcoona Quartzite.		No soil
RSP16-001	Y	Y	0715113 E 6627457 N	CHep ₃	LMC	5 Yr 4/6	5-5.5	Silcrete, goethite, gypsum, blocky quartzite with muscovite grains, and small rounded pebbles.	Chenopods	Granular soil fragments observed ontop of mud cracks at surface
RSP16-002	Y	Y	0715096 E 6627431 N	Aed ₁	S	5 Yr 5/6	6			
RSP17-001	Y	Y	0714771 E 6627124 N	Ceh ₁	SC	5 Yr 4/6	7	Rounded fluvial pebbles, sub-rounded quartzite, silcrete, angular sandstone and ferruginous nodules.	Bluebush, senna, saltbush, grasses	

Sample	Soil	Lag	Location	Landform	Texture	Colour	pH	Lag	Vegetation	Extra Notes
RSP18-001	Y	Y	0707475 E 6626278 N	CHep ₁	SCL	5 Yr 5/6	8.5	Varying grain shape and sizes of silcrete (jasper), quartzite, small hematite angular nodules, rounded quartz fragments, silicified conglomerates with small rounded quartz clasts and potch opal closer to opal diggings.	Bluebush	
RSP19-001	Y	Y	0709838 E 6623119 N	CHep ₁	SC	5 Yr 5/8	7	Varying grain shape and sizes of silcrete (jasper), quartzite, small hematite angular nodules, rounded quartz fragments, silicified conglomerates with small rounded quartz clasts and potch opal closer to opal diggings.	Pearl bluebush	

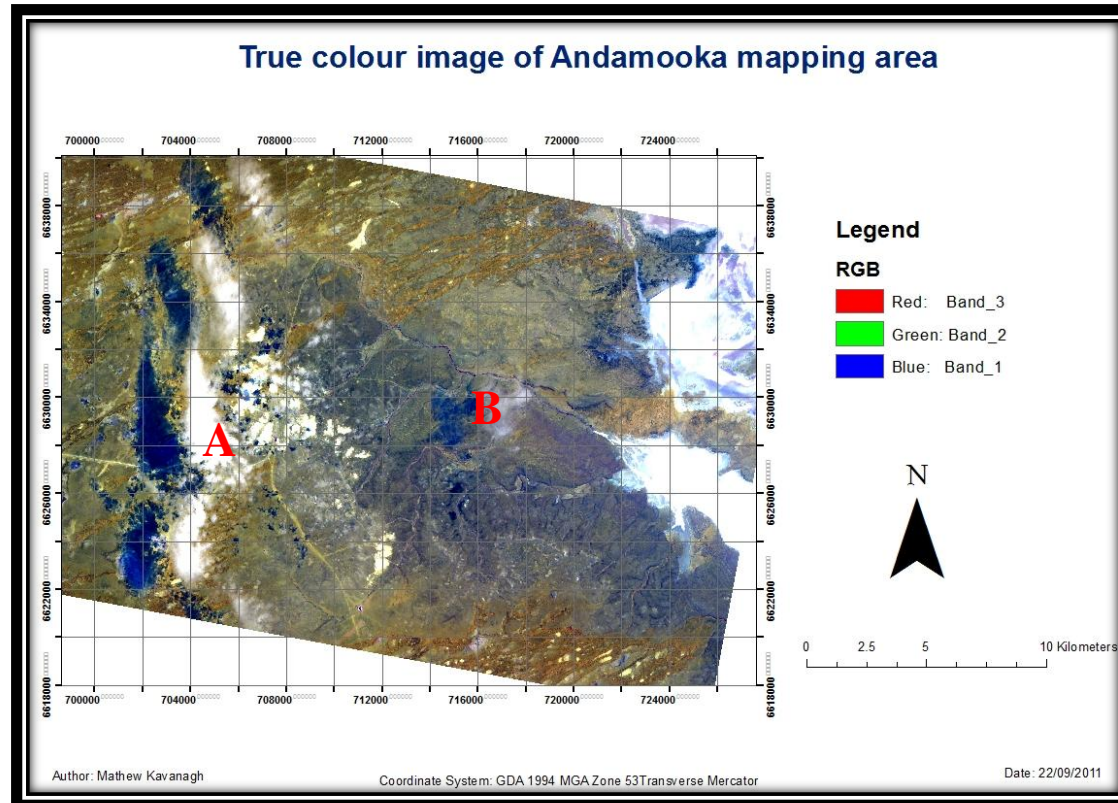
Appendix 2

Digital elevation model (using SRTM values) of Andamooka mapping area showing interpreted position of current opal digging boundaries (red outline)



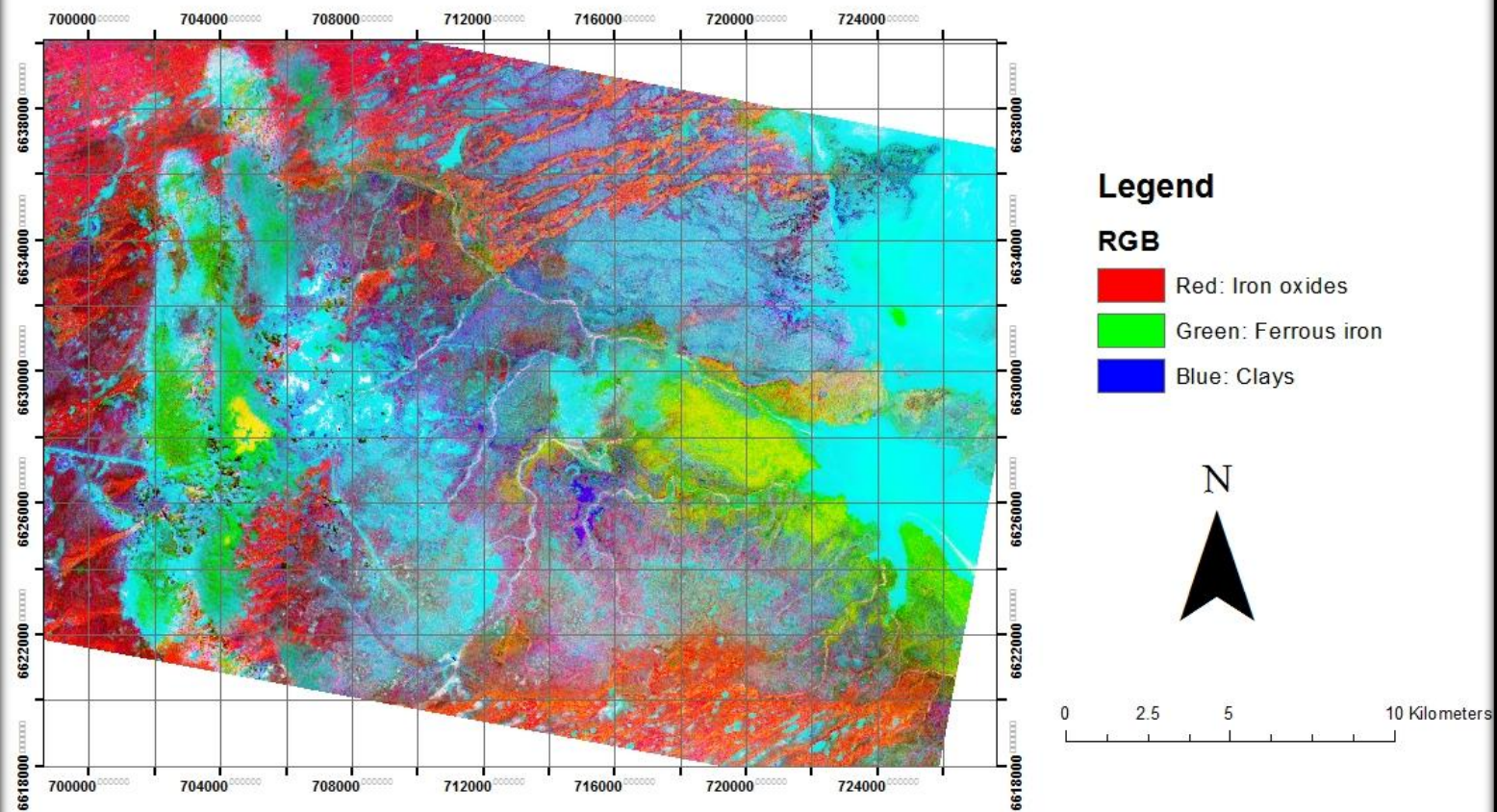
Appendix 3

ASTER band ratio images



True colour image for the Andamooka Mapping area. Important to note the presence of dense cloud cover to the west (a) and light cloud cover to the east (b) and their cloud shadows. These clouds and shadows will ultimately affect the processed ASTER images and hence should be ignored.

CSIRO regolith ratios



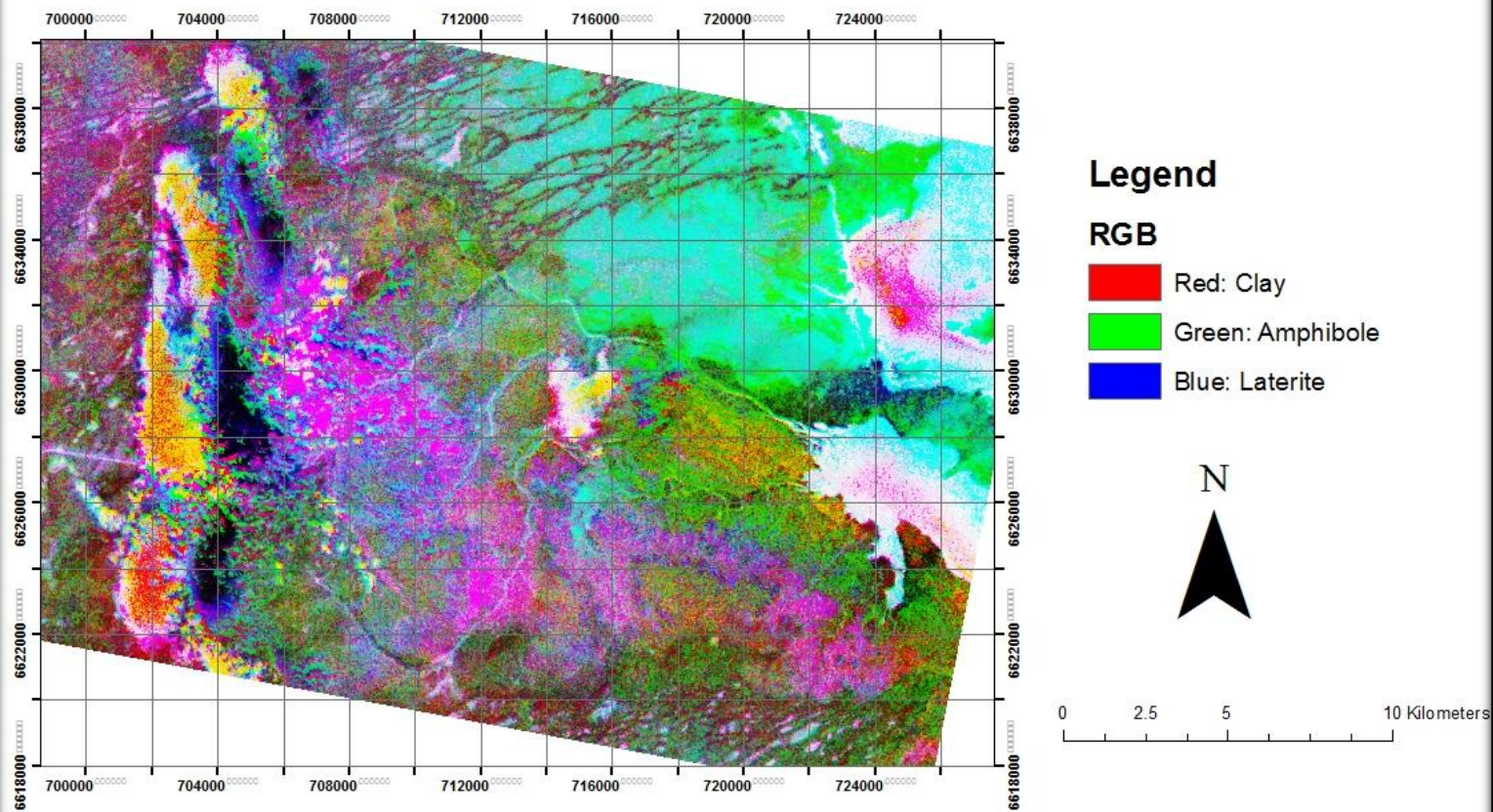
Author: Mathew Kavanagh

Coordinate System: GDA 1994 MGA Zone 53 Transverse Mercator

Date: 22/09/2011

Red: Iron Oxides (B3/B2), Green: Ferrous iron i.e. non-mafic rocks (B3/B7), Blue: Clays (B4/B7)

Band ratios highlighting clay, amphibole and laterite content



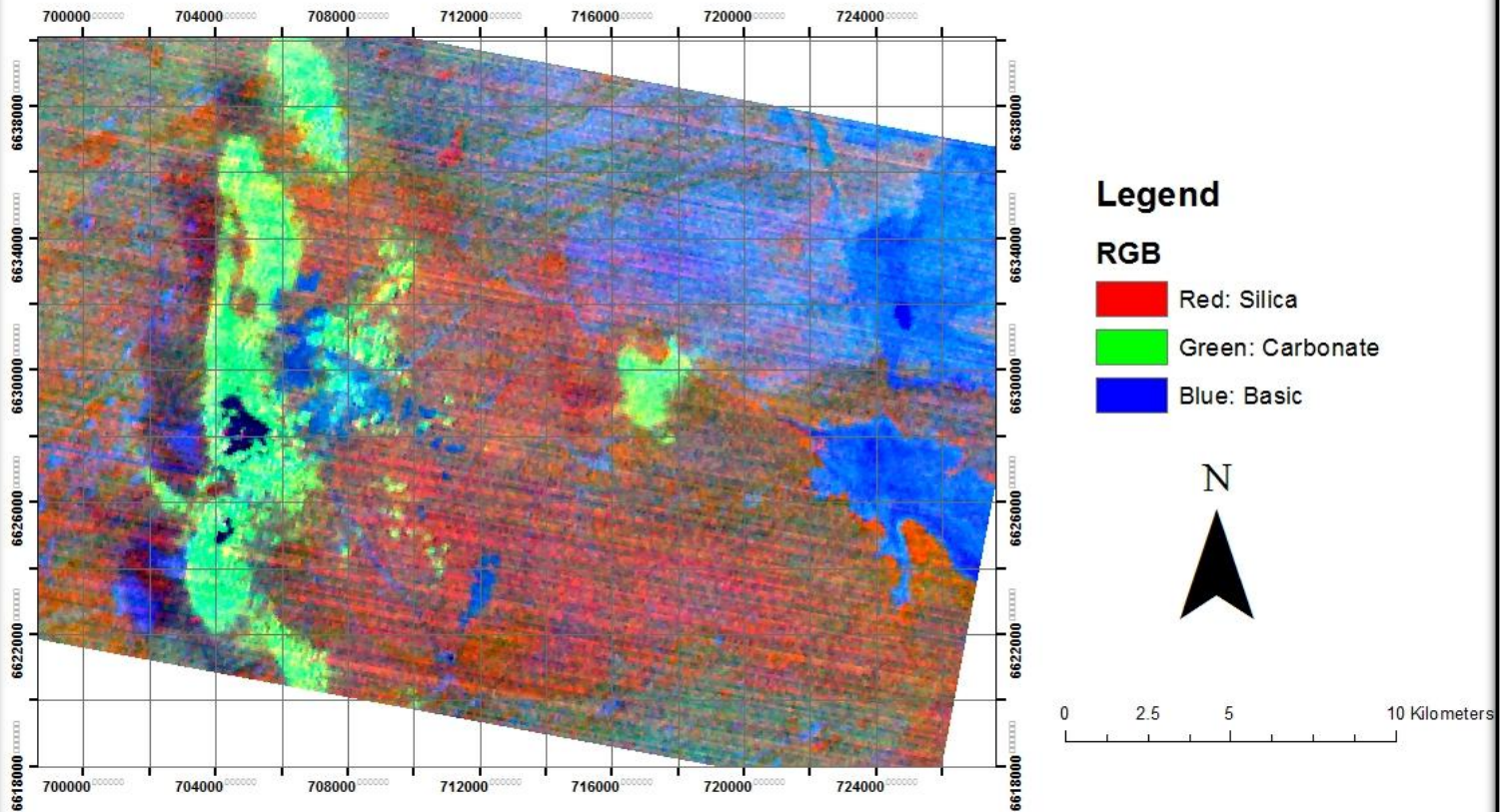
Author: Mathew Kavanagh

Coordinate System: GDA 1994 MGA Zone 53 Transverse Mercator

Date: 22/09/2011

Red: Clay $((B5 \times B7) / B6^2)$, Green: Amphibole $(B6 / B8)$, Laterite $(B4 / B5)$

Band ratios highlighting silica, carbonate and basic content



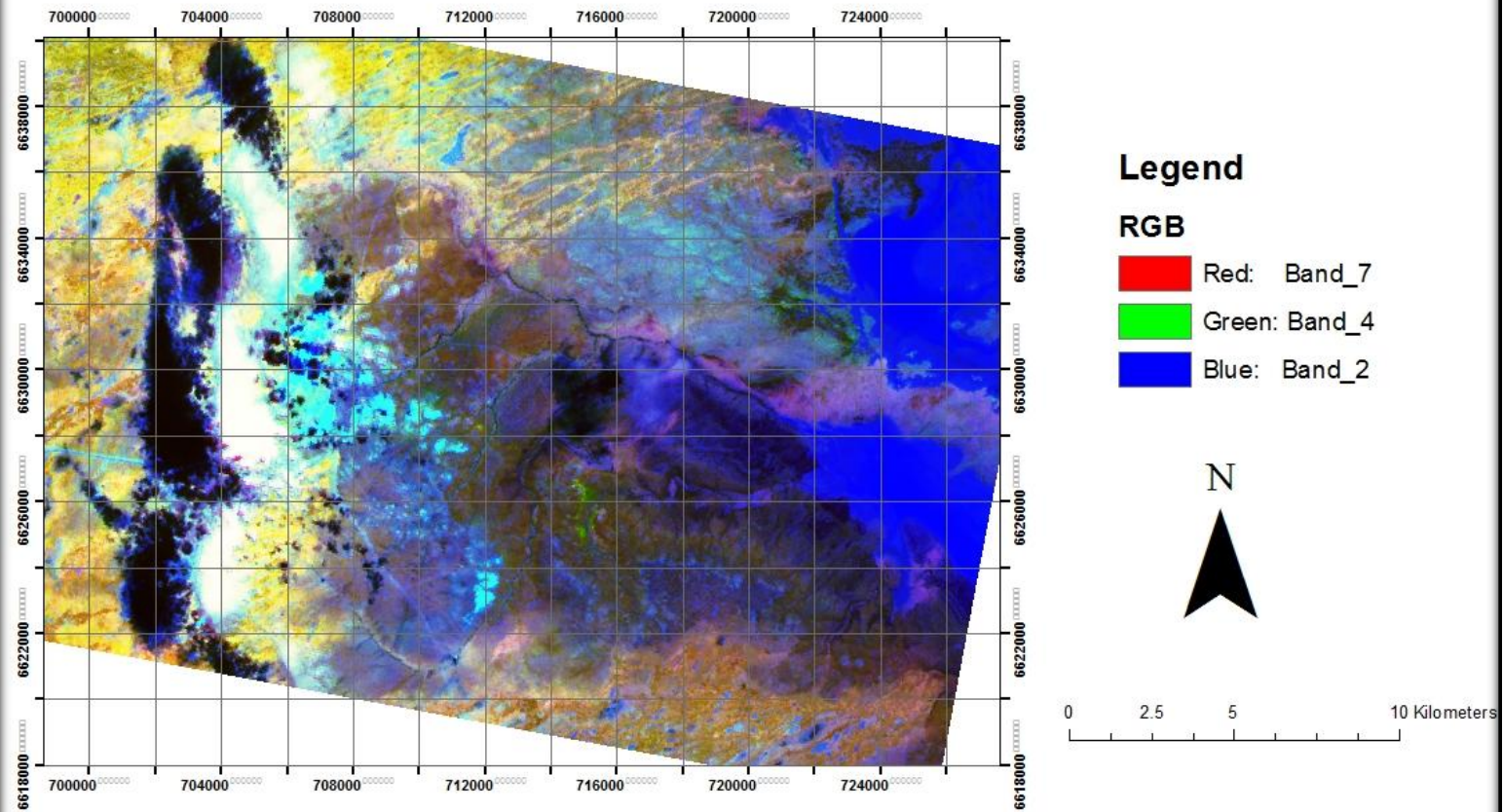
Author: Mathew Kavanagh

Coordinate System: GDA 1994 MGA Zone 53 Transverse Mercator

Date: 22/09/2011

Red: Silica ((B11x B11)/B10/B12), Green: Carbonate (B13/B14), Blue: Basic (B12/B13)

Band combination enhancing structural features



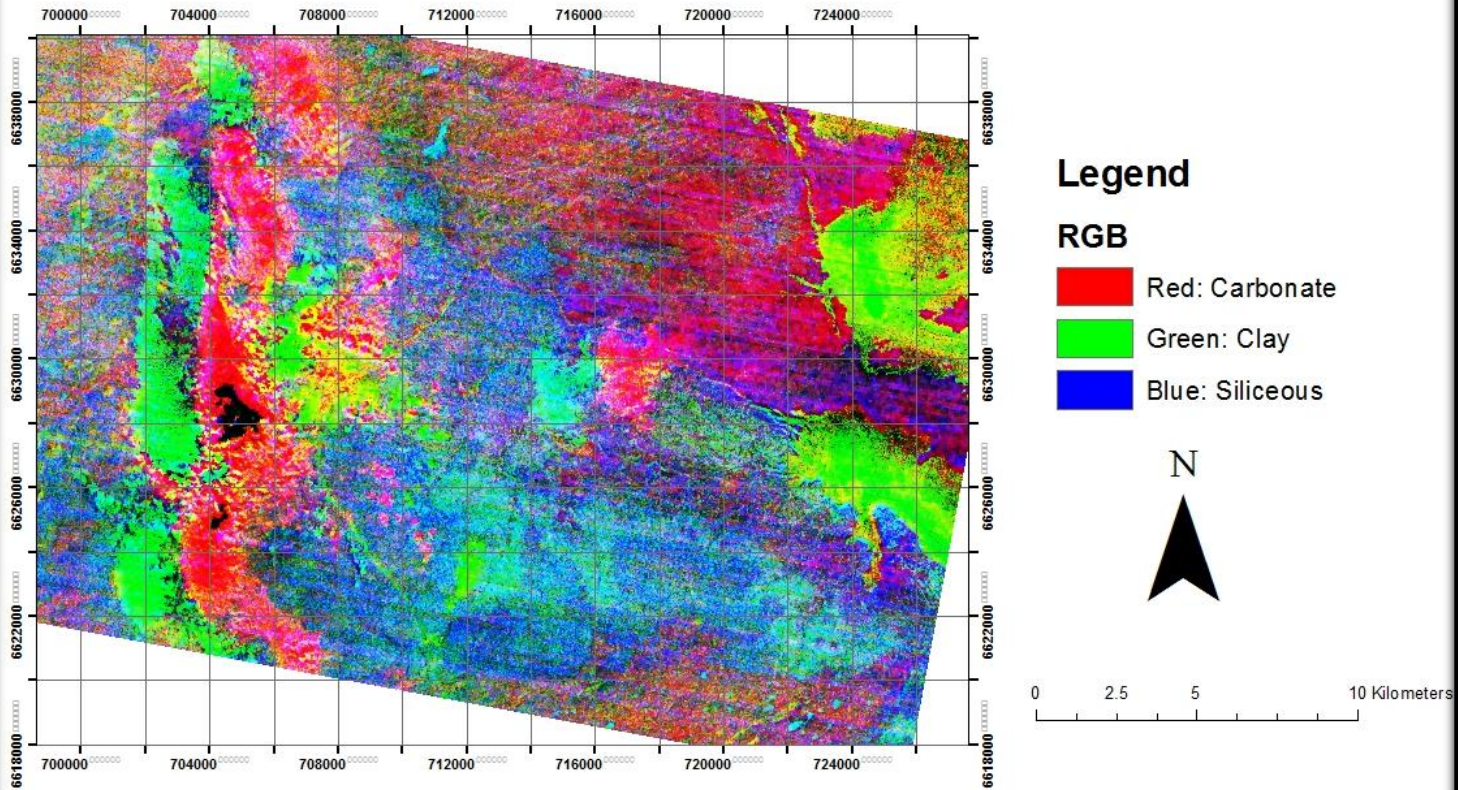
Author: Mathew Kavanagh

Coordinate System: GDA 1994 MGA Zone 53 Transverse Mercator

Date: 22/09/2011

Red: B7, Green: B4, Blue: B2

Band ratios highlighting carbonate, clay and siliceous content



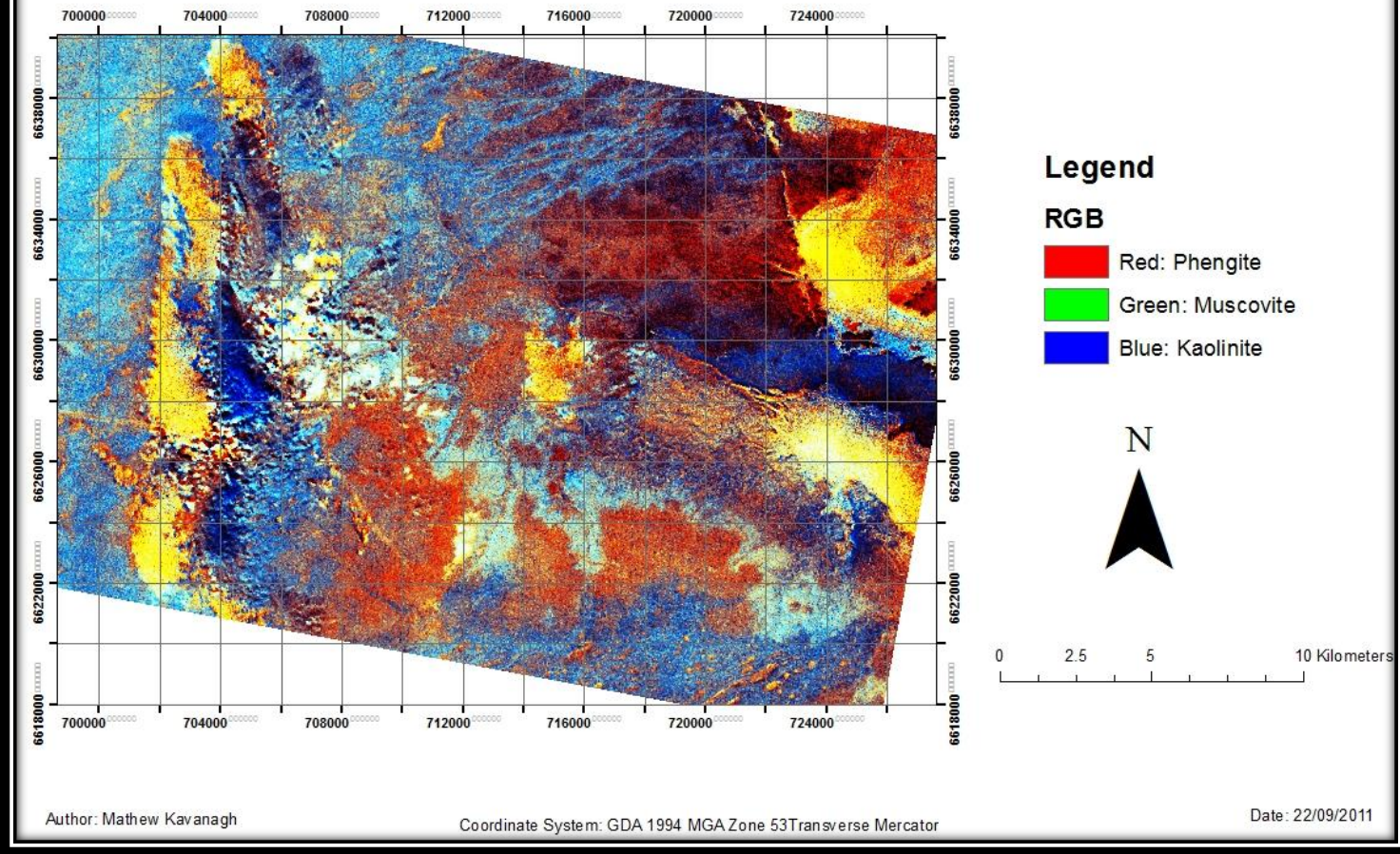
Author: Mathew Kavanagh

Coordinate System: GDA 1994 MGA Zone 53 Transverse Mercator

Date: 22/09/2011

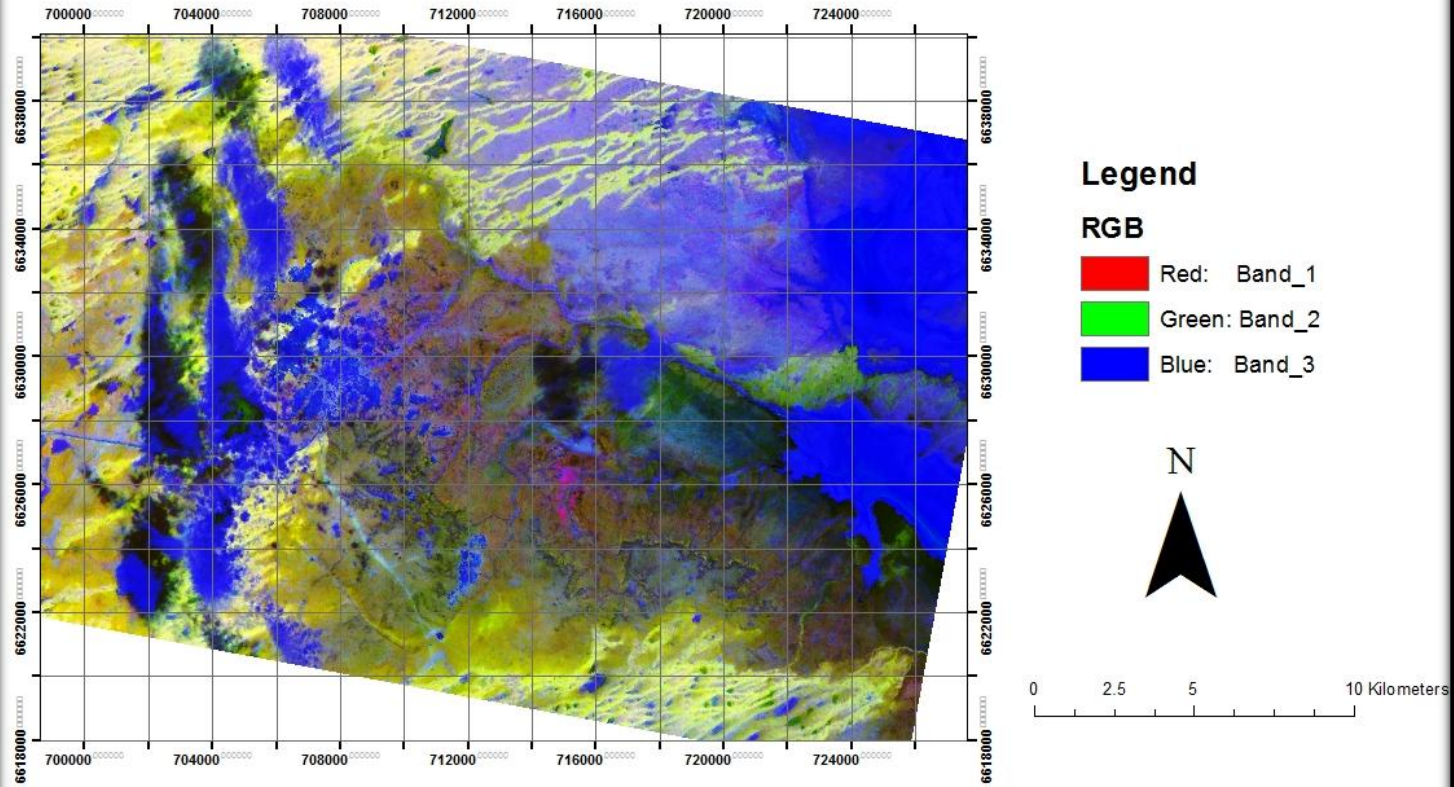
Red: Carbonate ($B13/B14$), Green: Clay ($(B5 \times B7)/6^2$), Blue: Siliceous ($(B11 \times B11)/(B10/B12)$)

Band ratios highlighting Al-OH content



Red: Phengite (B5/B6), Green: Muscovite (B7/B6), Blue: Kaolinite (B7/B5)

Band ratios highlighting areas of discrimination for mapping



Author: Mathew Kavanagh

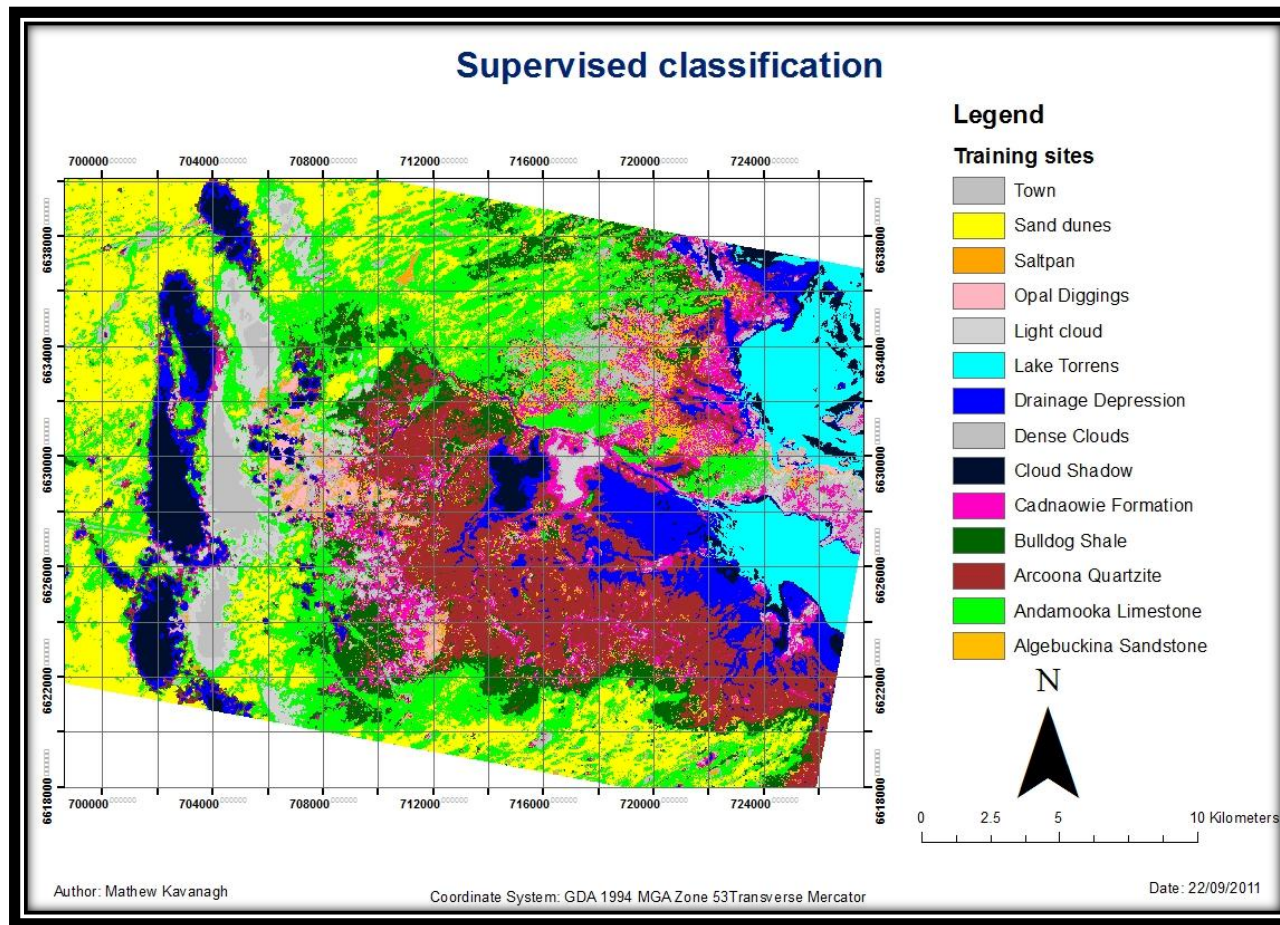
Coordinate System: GDA 1994 MGA Zone 53 Transverse Mercator

Date: 22/09/2011

Red: B4/B1, Green: B3/B1, Blue: B12/B14

Appendix 4

Supervised classification (minimum distance to mean)



Supervised Classification performed in ERDAS Imagine, using field observations and sample locations as training sites to distinguish average spectral signatures for the defined classes.

Appendix 5

Processed Hylogger Data showing main minerals predicted from the SWIR and VNIR spectrums

	Minerals Present (SWIR)	Dominant Mineral (VNIR)
RSP1-001 sample (Lag)		
1	Muscovite, Kaolinite PX, Siderite, Aspectral, Magnesite, Montmorillonite	Goethite-2
2	Aspectral, Siderite	Goethite-2
3	Aspectral, Siderite, Kaolinite PX	
4	Kaolinite PX	Hematite
5	Montmorillonite	
6	Kaolinite PX, Muscovite	
Avg	Kaolinite PX (21%), Dickite (2%), Muscovite (46%), Montmorillonite (9%), Magnesite (4%), Siderite (28%), Aspectral (28%)	Hematite (20%), Goethite-2 (90%)
RSP1-002 sample (Lag)		
1	Kaolinite PX, Siderite, Aspectral, Muscovite, Palygorskite	
2	Montmorillonite	
3	Montmorillonite, Siderite, Aspectral	
4	IlliticPhengite, Phengite, Kaolinite PX, Magnesite, Montmorillonite, Aspectral	
5	Kaolinite WX, Dickite, Kaolinite PX	
Avg	Kaolinite WX (7%), Kaolinite PX (37%), Muscovite (8%), Montmorillonite (50%), Dolomite (10%), Magnesite (28%), Siderite 13%), Aspectral (2%)	
RSP2-001 sample (Lag)		
1	Kaolinite WX, Kaolinite PX, Montmorillonite	Hematite, Goethite-2
2		Goethite-2
3	Kaolinite WX, Kaolinite PX	
Avg	Kaolinite WX (75%), Kaolinite PX (24%), Muscovite (13%), Montmorillonite (6%)	Hematite (69%), Goethite-2 (100%)

<i>(cont.)</i>	Minerals Present (SWIR)	Dominant Mineral (VNIR)
RSP2-002 sample (Lag)		
1	Kaolinite PX, Siderite, Dickite, Aspectral, Kaolinite WX	
2		
3	Kaolinite WX, Kaolinite PX	
4	Kaolinite WX	
5	Kaolinite WX, Kaolinite PX	
Avg	Kaolinite WX (38%), Kaolinite PX (59%), Muscovite (11%), Montmorillonite (1%), Magnesite (1%), Siderite (5%), Gypsum (7%), Jarosite (5%)	
RSP2-003 sample (Lag)		
1	Montmorillonite, Aspectral	
2		
3	Kaolinite PX, Siderite, Aspectral, Muscovite	
4	Siderite	
5	Illitic Muscovite, Phengite, Montmorillonite, Siderite, Muscovite	Goethite-2
Avg	Kaolinite PX (2%), Muscovite (2%), Montmorillonite (89%), Dolomite (5%), Magnesite (72%), Siderite (13%), Aspectral (5%)	Goethite-2 (75%)
RSP3-001 sample (Lag)		
1	Muscovite, Illitic Muscovite, Kaolinite PX, Kaolinite WX	
2		
3		
4	Muscovite, Aspectral, Kaolinite PX, Siderite	Goethite-2
5	Magnesite, Muscovite	Hematite
Avg	Kaolinite WX (22%), Kaolinite PX (41%), Muscovite (29%), Montmorillonite (16%), Siderite (3%), Aspectral (29%)	Hematite (69%), Goethite-2 (96%)
RSP4-001 sample (Lag)		
1		
2	Calcite, Ankerite	
Avg	Palygorskite (100%), Calcite (66%), Ankerite (33%)	

<i>(cont.)</i>	Minerals Present (SWIR)	Dominant Mineral (VNIR)
RSP5-001 sample (Lag)		
1	Aspectral, Siderite, Illitic Muscovite, Muscovite,	
2	Siderite, Kaolinite PX, Kaolinite WX	
3	Kaolinite PX	
4		
5		
6	Kaolinite PX, Aspectral	Hematite, Goethite-2
7	Kaolinite PX	
8	Kaolinite WX	Hematite
Avg	Kaolinite WX (9%), Kaolinite PX (36%), Muscovite (6%), Montmorillonite (9%), Siderite (3%), Aspectral (45%)	Hematite (50%), Goethite-2 (25%)
RSP6-001 sample (Lag)		
1	Montmorillonite	Goethite-2
2	Aspectral	Goethite-2
3	Montmorillonite, Siderite, Aspectral	Hematite, Goethite
4	Siderite, Aspectral	
Avg	Kaolinite PX (12%), Montmorillonite (75%), Palygorskite (50%), Aspectral (18%)	Hematite (22%), Goethite-2 (77%)
RSP8-001 sample (Lag)		
1	Kaolinite PX, Kaolinite WX, Muscovite	
2	Muscovite, Kaolinite PX, Kaolinite WX, Montmorillonite	Hematite
Avg	Kaolinite WX (30%), Kaolinite PX (69%), Muscovite (40%), Montmorillonite (8%), Illitic Muscovite (1%)	Hematite (100%), Goethite-2 (100%)
RSP10-002 sample (Lag)		
1	Kaolinite PX, Kaolinite WX	Hematite, Goethite-2
2	Kaolinite PX, Siderite	Goethite-2
Avg	Kaolinite PX (34%) & WX (63%), Muscovite (36%), Montmorillonite (7%), Seridite (2%), Illitic muscovite (10%)	Hematite (86%), Goethite-2 (100%)

<i>(cont.)</i>	Minerals Present (SWIR)	Dominant Mineral (VNIR)
RSP11-001 sample (Lag)		
1	Aspectral, Kaolinite PX, Siderite	
2	Kaolinite PX, Siderite	
3	Kaolinite PX, Siderite	
Avg	Kaolinite Px (57%), Muscovite (12%), Montmorillonite (12%), Magnesite (7%), Siderite (25%), Aspectral (17%)	
RSP12-001 sample (Lag)		
1	Kaolinite WX, Kaolinite PX	
2	Magnesite, Montmorillonite, Siderite, Aspectral, Kaolinite PX	Goethite-2
3	Kaolinite WX	
4	Kaolinite WX	Hematite
5	Kaolinite WX	
6	Aspectral	Goethite-2
Avg	Kaolinite WX (70%), Kaolinite PX (20%), Muscovite (20%), Montmorillonite (49%), Magnesite (1%), Siderite (4%), Aspectral (3%), Illitic Muscovite (7%)	Hematite (16%), Goethite-2 (96%)
RSP13-001 sample (Lag)		
1	Muscovite, Kaolinite PX, Aspectral, Siderite	Goethite-2
2	Aspectral	Goethite-2, Goethite-1
3	Aspectral, Siderite	Goethite-2
Avg	Kaolinite PX(4%), Muscovite (5%), Siderite (4%), Aspectral (89%)	Goethite2 (58%), Goethite-1 (2%)
RSP13-002 sample (Lag)		
1	Kaolinite PX, Siderite, Magnesite, Kaolinite WX	Goethite-2
2	Aspectral	Goethite-2
3	Kaolinite WX, Kaolinite PX, Montmorillonite, Aspectral	Hematite, Goethite-1, Goethite-2
4	Siderite, Kaolinite PX	
5	Kaolinite WX	
Avg	Kaolinite WX (59%), Kaolinite PX (19%), Muscovite (1%), Montmorillonite (72%), Magnesite (4%), Siderite (17%), Aspectral (3%), illitic Muscovite (1%)	Hematite (61%), Goethite-2 (77%), Goethite-1 (22%)

<i>(cont.)</i>	Minerals Present (SWIR)	Dominant Mineral (VNIR)
RSP14-001 sample (Lag)		
1	Aspectral, Kaolinite PX, Muscovite, Montmorillonite	Goethite-2
2	Aspectral, Kaolinite WX, Kaolinite PX	Hematite
3	Aspectral, Kaolinite PX, Muscovite, Siderite	Goethite-2
4	Aspectral	Goethite-2
5	Siderite, Kaolinite PX, Muscovite, Aspectral	Goethite-2
Avg	Kaolinite WX (17%), Kaolinite PX (21%)Muscovite (30%), Montmorillonite (1%)Siderite (2%), Gypsum (1%), Aspectral (52%)	Hematite (20%), Goethite-2 (38%)
RSP15-001 sample (Lag)		
1		
2	Aspectral, Montmorillonite, Palygorskite, Nontronite	
Avg	Montmorillonite (14%), Nontronite (17%), Palygorskite (14%), Aspectral (70%)	Goethite-2 (100%)
RSP16-001 sample (Lag)		
1		
2		
3	Aspectral	Hematite
4	Kaolinite WX, Montmorillonite, Muscovite, Kaolinite PX, Aspectral	Goethite-2, Hematite
5	Kaolinite PX, Montmorillonite, Kaolinite WX	
6	Aspectral	Goethite-2
Avg	Kaolinite WX (7%), Kaolinite PX (36%), Muscovite (4%), Montmorillonite (14%), Gypsum (1%), Dry Vegetation (1%), Aspectral (50%)	Hematite (4%), Goethite-2 (46%)
RSP16-002 sample (Lag)		
1	Kaolinite PX, Muscovite, Siderite, Aspectral	Goethite-2
2	Montmorillonite, Kaolinite PX, Muscovite, Kaolinite WX	Goethite-2
3		
4		Goethite-2
5	Aspectral	Goethite-2
Avg	Kaolinite WX (28%), Kaolinite PX (15%), Muscovite (6%)	Hematite (56%) Goethite-2 (100%)

<i>(cont.)</i>	Minerals Present (SWIR)	Dominant Mineral (VNIR)
RSP17-001 sample (Lag)		
1	Montmorillonite	
2	Montmorillonite, Kaolinite PX	
3	Montmorillonite	
4		
5	Montmorillonite	
6	Kaolinite WX, Kaolinite PX	
7		
Avg	Kaolinite WX (7%), Kaolinite PX (36%), Muscovite (10%), Montmorillonite (63%), Dolomite (4%), Magnesite (26%), Sideriet (10%), Gypsum (7%)	
RSP18-001 sample (Lag)		
1	Siderite, Montmorillonite	Hematite, Goethite-2
2	Siderite, Kaolinite PX, Kaolinite Wx	
3		
Avg	Kaolinite PX (41%) & WX (33%), Muscovite (41%), Montmorillonite (16%), Siderite (25%)	Hematite (33%), Goethite-2 (66%)
RSP19-001 sample (Lag)		
1	Siderite, Aspectral	
2		Goethite-2
3	Kaolinite PX, Montmorillonite	Goethite-2
4	Kaolinite PX, Siderite	
5		Goethite-2
Avg	Kaolinite PX (61%), Montmorillonite (30%), Siderite (23%), Aspectral (15%)	Hematite (22%), Goethite-2 (88%)

Sample (Soil)	Minerals Present (SWIR)	Dominant Mineral (VNIR)
RSP1-001	Montmorillonite, Dickite, Kaolinite WX	
RSP1-002	Montmorillonite, Kaolinite WX	
RSP2-001	Kaolinite WX	Hematite
RSP2-002	Kaolinite WX	
RSP2-003	Montmorillonite	
RSP3-001	Montmorillonite	
RSP4-001	Palygorskite, Montmorillonite	
RSP5-001	Montmorillonite, Kaolinite WX	
RSP6-001	Montmorillonite, Palygorskite, Kaolinite Px	
RSP7-001	Montmorillonite, Kaolinite WX, Kaolinite PX	
RSP8-001	Montmorillonite, Kaolinite PX	
RSP9-001	Montmorillonite, Kaolinite PX, Kaolinite WX	
RSP10-001	Montmorillonite, Kaolinite PX, Kaolinite WX	
RSP10-002	Montmorillonite, Kaolinite WX	
RSP11-001	Montmorillonite, Kaolinite WX	
RSP12-001	Montmorillonite, Kaolinite WX	
RSP13-001	Montmorillonite, Kaolinite PX, Wood	
RSP13-002	Kaolinite WX, Montmorillonite	
RSP14-001	Muscovite, Kaolinite PX, Montmorillonite	
RSP16-001	Montmorillonite, Kaolinite PX, Kaolinite WX	
RSP16-002	Montmorillonite, Kaolinite PX, Kaolinite WX	
RSP17-001	Montmorillonite, Kaolinite PX	Goethite-2
RSP18-001	Montmorillonite, Kaolinite PX, Palygorskite	
RSp19-001	Montmorillonite	